SANDIA REPORT
SAND2012-8110
Unlimited Release
Printed September 2012

EFFECTS OF DEFECTS IN COMPOSITE WIND TURBINE BLADES: ROUND 1

Jared W. Nelson, Trey W. Riddle, and Douglas S. Cairns (Principal Investigator)
Department of Mechanical & Industrial Engineering
Montana State University, Bozeman, MT

Sandia Technical Manager: Joshua A. Paquette

Prepared by
Sandia National Laboratories
Albuquerque, New Mexico 87185 and Livermore, California 94550

Sandia National Laboratories is a multi-program laboratory managed and operated by Sandia Corporation, a wholly owned subsidiary of Lockheed Martin Corporation, for the U.S. Department of Energy's National Nuclear Security Administration under contract DE-AC04-94AL85000.

Issued by Sandia National Laboratories, operated for the United States Department of Energy by Sandia Corporation.

Available to DOE and DOE contractors from
U.S. Department of Energy
Office of Scientific and Technical Information
P.O. Box 62
Oak Ridge, TN 37831

Telephone: (865) 576-8401
Facsimile: (865) 576-5728
E-Mail: reports@adonis.osti.gov
Online ordering: http://www.osti.gov/bridge

Available to the public from
U.S. Department of Commerce
National Technical Information Service
5285 Port Royal Rd.
Springfield, VA 22161

Telephone: (800) 553-6847
Facsimile: (703) 605-6900
E-Mail: orders@ntis.fedworld.gov
Online order: http://www.ntis.gov/help/ordermethods.asp?loc=7-4-0#online

SAND2012-8110
Unlimited Release
Printed September 2012

Effects of Defects in Composite Wind Turbine Blades: Round 1

Jared W. Nelson, Trey W. Riddle, and Douglas S. Cairns (Principal Investigator)
Department of Mechanical & Industrial Engineering
Montana State University, Bozeman, MT

Sandia Technical Manager: Joshua A. Paquette

Abstract

The Wind Turbine Blade Reliability Collaborative (BRC) was formed with the goal of improving wind turbine blade reliability. Led by Sandia National Laboratories (SNL), the BRC is made up of wind farm maintenance companies, turbine manufacturers and third party investigators. Specific tasks have been assigned by SNL to the various parties. The portion of the BRC that will focus on establishing the criticality of manufacturing defects (aka, Effect of Defects) is being researched by the Montana State University Composites Group (MSUCG). The research described herein compiles the second round of a multi-year year plan consisting of three rounds of work performed by Montana State University (MSU) within two areas—Flaw Characterization and Effects of Defects. The purpose of this document is to capture and convey the progress which has been made by the MSU team under the first round of the effort.

The work presented has established that characterization of defects common to wind turbine blades is possible. A consistent framework has been established and validated for quantitative categorization and analysis of flaws. With proper characterization, it is possible to establish the structural implication of a flaw. Applying the characterization techniques described herein to incoming data will enable the generation of a statistically significant and comprehensive flaw database. It is the goal of this investigation that these tools and data, once disseminated to industry, will contributed to improvements in the reliability of wind turbines.

Understanding the changes in the material properties associated with characterized flaws has been achieved on a coupon level with physical testing being performed with several configurations of several different flaw types. This testing clearly indicated that fiber misalignment and porosity resulted in degraded material properties and decreased material performance. To complement and work toward predicting these types of results, simple modeling efforts have been performed and reasonable agreement has been achieved when compared to the test data. Additional work is necessary to improve the accuracy and a more complex modeling effort will be undertaken in the future.

Work will continue with efforts to acquire as-built flaw data to ensure the characterized flaws are representative of full-scale wind turbine blades. In addition, research will be performed into reliability methods suitable for wind turbine composites. Finally, characterization of second round test specimens for use in model validation and physical testing correlation through the use of improved and more accurate models.

Acknowledgements

The authors wish to acknowledge the help from Sandia contract monitors Dr. Daniel Laird (through March, 2011) and Mr. Joshua Paquette (current). The authors also wish to acknowledge technical help from Mr. Tom Ashwill , Mr. Mark Rumsey, Dr. Dennis Roach, and Mr. Kirk Rackow of Sandia National Laboratories, in conjunction with the Wind Energy Technology Department.

Table of Contents

List of Figures

List of Tables

I. Introduction

The size, weight, shape, operational environment, and economic considerations of wind turbine blades have essentially dictated the use of low cost composites materials and manufacturing methods. Even though composites have superior engineering qualities, it is not apparent that design and manufacturing within the wind industry are able ensure a 20-year product life.[1] Prevention of failures has a profound economic impact on the continued development of the wind turbine industry.[2] While significant research has been performed to better understand what is needed to improve blade reliability, a comprehensive study to characterize and understand the manufacturing flaws commonly found in blades has not been performed.[1,3,4] The Blade Reliability Collaborative (BRC) sponsored by the U.S. Department of Energy (DOE) and led by Sandia National Laboratories (SNL) has been formed to perform such research.[5]

The function of the Flaw Characterization portion of this program has been to provide quantitative analysis for two major directives; (1) acquisition & generation of quantitative flaw data for use in the Effects of Defects numerical modeling program and (B) development of a flaw severity designation system for as built flaws. The Effects of Defects portion is focused on the development of modeling capabilities to predict the structural implications of common flaws found in composite wind turbine blades.

II. Flaw Characterization

The preliminary results from a survey of wind turbine blade manufactures, repair companies, wind farm operators and third party investigators has directed the focus of this investigation on two types of flaws commonly found in wind turbine blades: waviness and porosity/voids.[20] A variety of flaw geometries as defined by in-field collection of production scale blade data has been investigated and complied. Basic statistical analysis has shown that the data generally follows standard distributions. The preliminary results from this effort and coupon level testing have established a protocol by which a defect in a blade can be characterized quantifiably. With this data and other parameters it is possible to develop criticality and probabilistic failure models that can be used to evaluate the risk of continued operation or deploying a flawed structure into service.

A. Wind Industry Blade Survey and Development of Flaw Database

The BRC has directed the MSU team to investigate the effects of porosity, in-plane (IP) and out-of-plane (OP) waves. It is critical to the development of this program to identify the precise geometric nature of these flaws based on statistical commonality in wind turbine blades. In order to do this, several commercial scale wind turbine blades were reviewed. To date, the data set has been limited to four blades which were reviewed for OP waves and one for IP waves. However, this data has provided a strong starting place for the analysis team and the development of a protocol by which other blades can be examined and their flaws characterized in the future.

i. Data Acquisition

The process by which IP wave, OP wave and adhesive joint data were collected was the same. Photographs of as-built flawed blade sections were taken. In the case of OP waves and adhesive bond lines, portions were cut out of blades to provide a cross-section view of the skin and spar cap laminates. This was not necessary for IP waves as those anomalies were visible on the unpainted surface. For all cases a measurement device was placed in the region of interest. The digital image was then imported

into Image J, an open source image processing software package typically used in the medical imaging field. In this environment the photos were converted to 8-bit color, and then the wave features were manually traced with a black line (Figure 1).

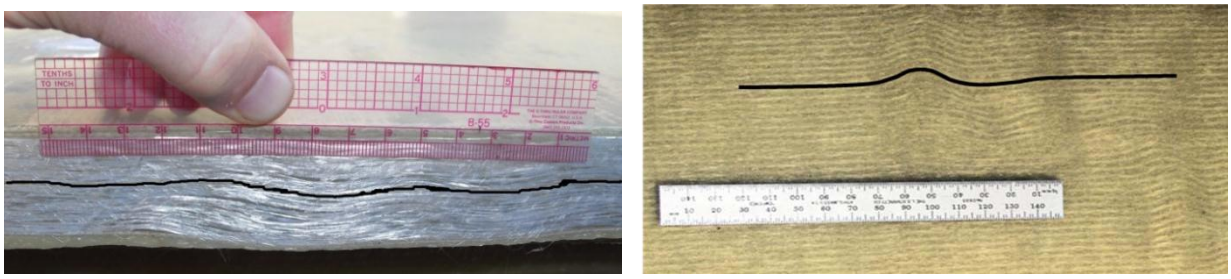

Figure 1: Image of OP wave (left) and IP wave (right).

The incorporation of the measurement device into the photo made it possible to develop a pixel based dimensioning system. This was the extent of the image processing necessary for the adhesive bondlines. Waveform flaw images required more processing. Colors in an 8-bit space are represented with a number from 0 (black) to 255 (white), enabling the application of mathematical operations to remove unwanted colors. Manipulating the color depth of each pixel allowed for the removal of the background, leaving only the feature tracing line. This image was then exported as a binary bitmap. A separate processing script was written in Matlab to extract the spatial coordinate data. From this data, each complete wave form was discretized into separate individual waveforms. One example of a complete wave and the waveform discretization process is shown in Figure 2.

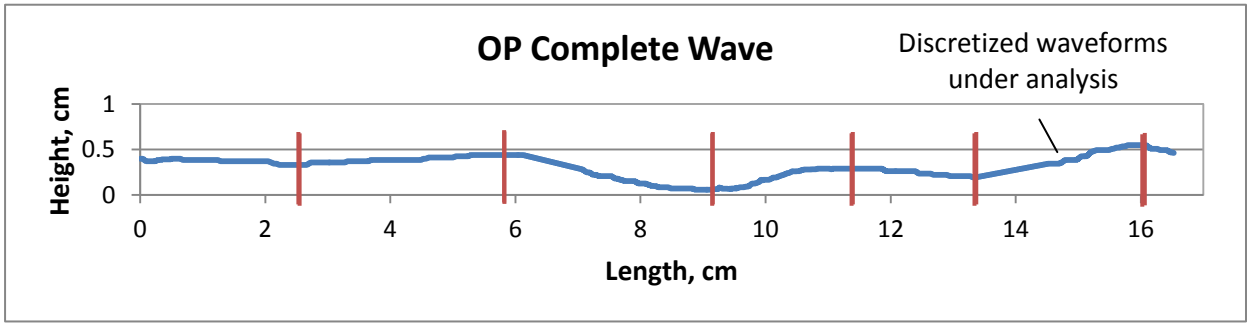

Figure 2: Example OP Wave. Complete spatial data and discretization positions.

Each discretized wave form's geometry was then mathematically characterized. Cubic splines and sinusoidal curve fits were both evaluated for applicability. Both techniques yielded similar goodness-of-fit tendencies. The sinusoidal analysis proved to be faster and was therefore chosen for utilization on the bulk data analysis. Once a fit was performed each wave was characterized in terms of wavelength, amplitude and off-axis fiber angle Figure 3. While, some previous studies have used aspect ratio instead of fiber angle as metric for characterization, such quantification may be slightly more challenging in the field. Aspect ratio requires knowing both the amplitude and wavelength whereas the fiber angle can be measure directly. [6,7]

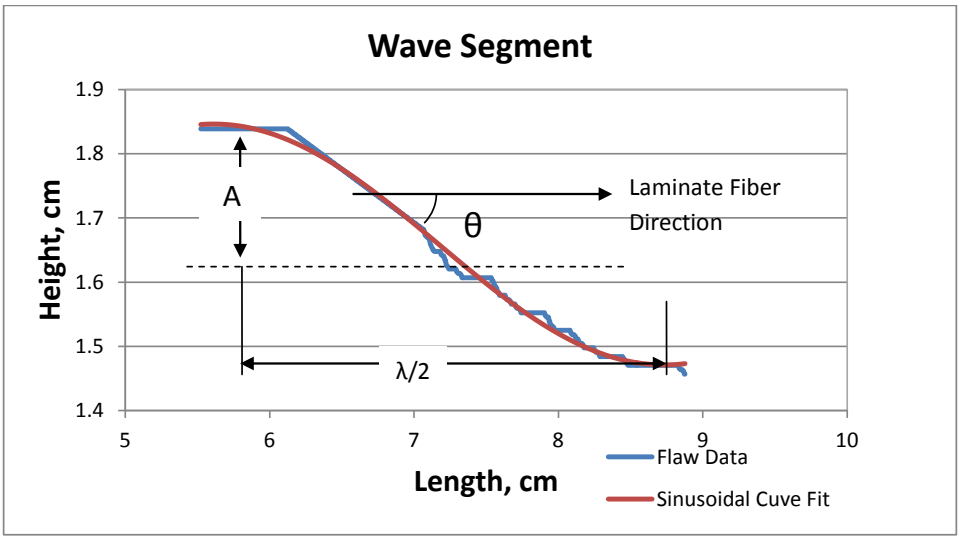

Figure 3: Example of sine wave fit, where A is the wave amplitude, λ is the wavelength and θ is the off-axis fiber angle.

After reviewing the same group of images for adhesive bondlines it has been inferred that there are two distinct cases where adhesives are used in wind turbine blades. For the purposes of this reporting, the two cases will be referred to as "Spar", where adhesives are used to bond the spar cap or shear web to the skin of the blade and "Mold Line" where adhesives are used to bond the two molded halves of the blade skin together. Representative images of the two cases are shown below in Figure 4.

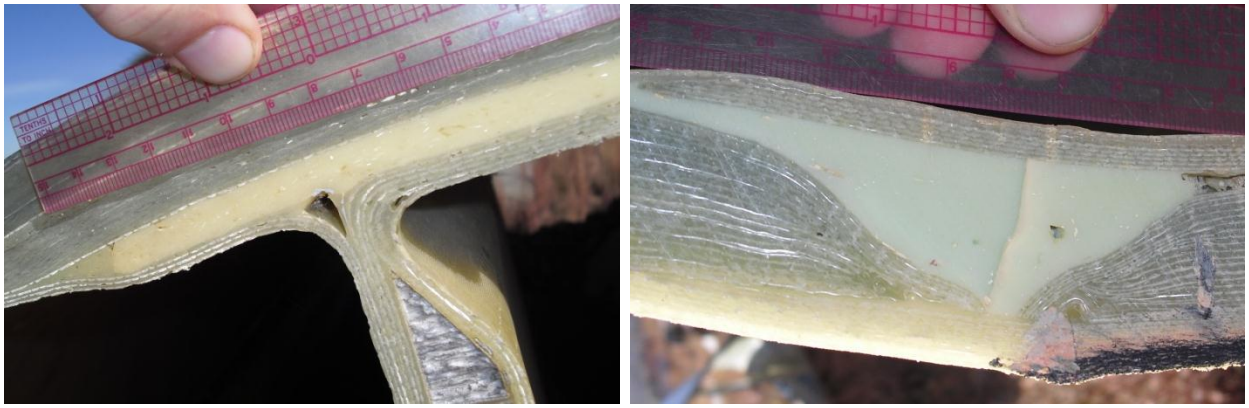

Figure 4: Spar to shear web adhesive bondline (left) and adhesive mold-line (right).

In both cases voids were found to be extremely prevalent, nearly ubiquitous. The general shape of voids tended to be elliptical. Moreover every image showed some porosity content as well. Bonding of the spar cap and shear web to the blade skin appeared fairly straight forward. Mold lines on the contrary exhibited a variety of negative manufacturing attributes. All mold line cases showed voids, some porosity, ply drops and in many cases extreme OP waves. Another artifact of the mold joining process was the use of laminate patches on either side of the joint for reinforcement.

In addition to identifying the function or type of adhesive application it is also necessary to define characterizing geometry such that an application can be quantitatively analyzed. Defining characteristics Figure 5 of the Spar case include; adhesive thickness, void dimensions and percent porosity.

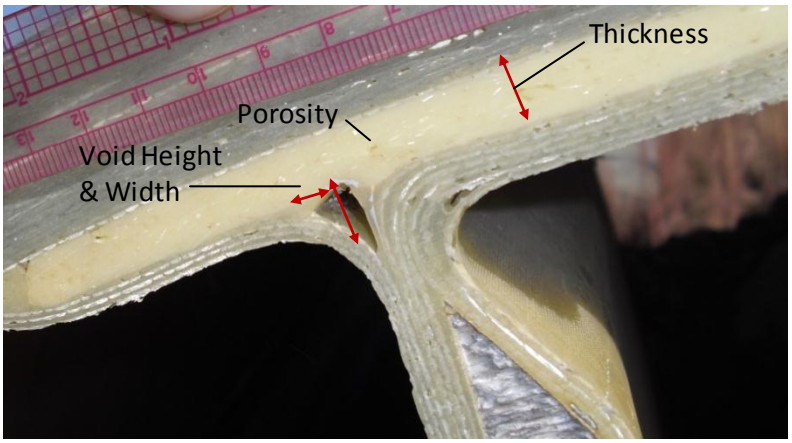

Figure 5: Spar case characterizing geometry.

Defining characteristics of the Mold Line Figure 6 case include; adhesive height & base, void dimensions (same as Spar), number of plies, ply drop height, ply drop length, ply drop aspect ratio. Based on the images collected, the porosity level proved difficult to obtain.

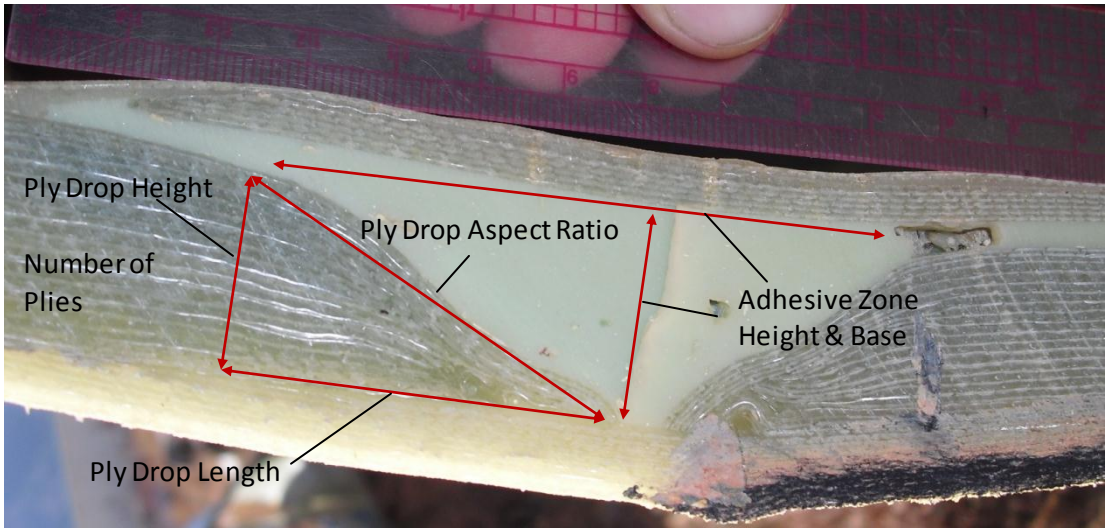

Figure 6: Mold line characterizing geometry.

ii. Data Analysis

Characterization of the various wave flaws found in the field data yielded 63 OP and 48 IP independent, discrete waveforms. Values for amplitude and wavelength of each instance are shown in Figure 7 and Figure 8. Here it can be seen that there is significant variation within the data. However, the data are well grouped indicating some consistency in the manufacturing processes. Of interest for this work are the outliers and statistical anomalies. The results of calculated off-axis fiber angles for OP waves and IP waves are shown in Figure 9 and Figure 10. Specific attention should be paid to the outlying group of angles highlighted by the red circle in Figure 9. Of particular note is that these angles were collected from blade sections which failed at these out-of-plane flaw locations.

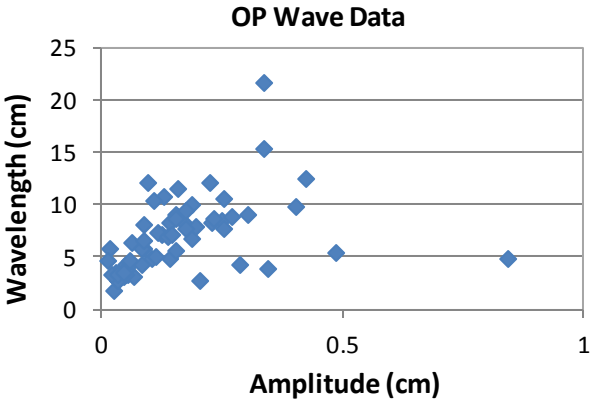

Figure 7: Collected OP wave data.

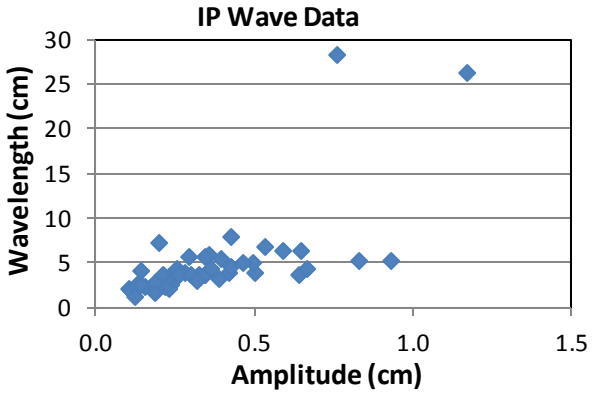

Figure 8: Collected IP wave data.

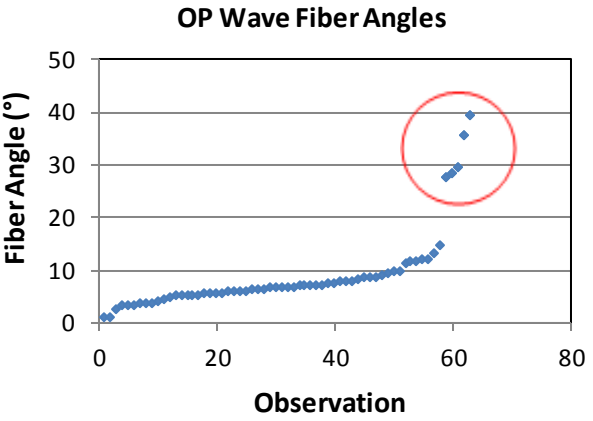

Figure 9: OP wave off-axis fiber angles.

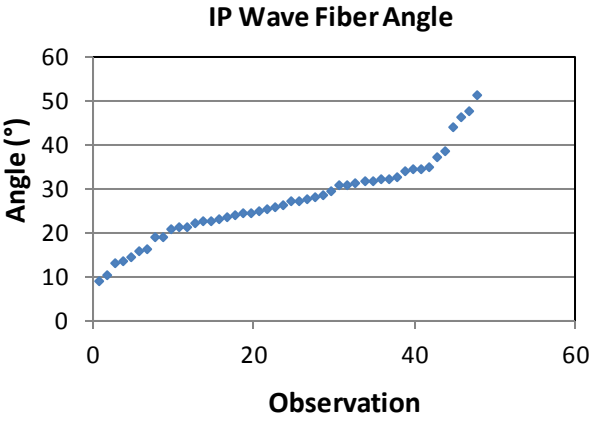

Figure 10: IP wave off-axis fiber angles.

In order to develop frequency of occurrences distributions, fiber angle values were grouped together. For the case of OP waves, angles were binned in one degree increments. IP wave angles were grouped in four degree increments. Binning of OP wave fiber angle values shows a strong inclination towards common distributions such as the Weibull and Normal distributions. This can be seen in Figure 11 where the observed frequency of occurrence is displayed with the distribution curves. It is interesting to note the IP wave fiber angle data did not follow such trends (Figure 12). This is most likely the result of a lack of source data for the IP waves.

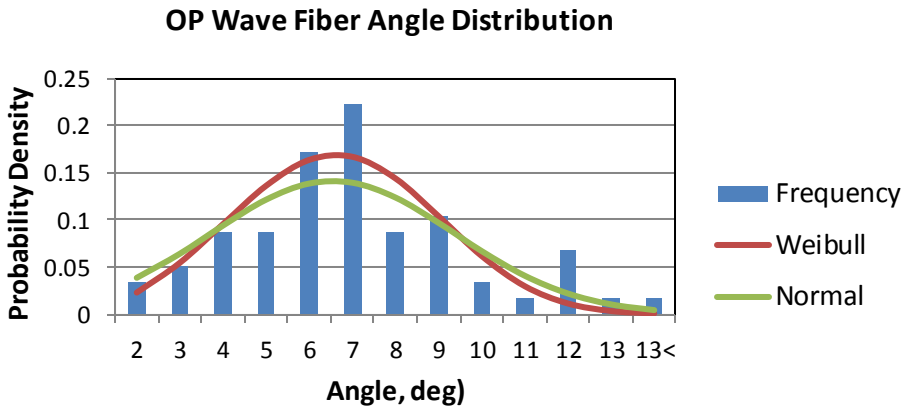

Figure 11: OP fiber angle distributions.

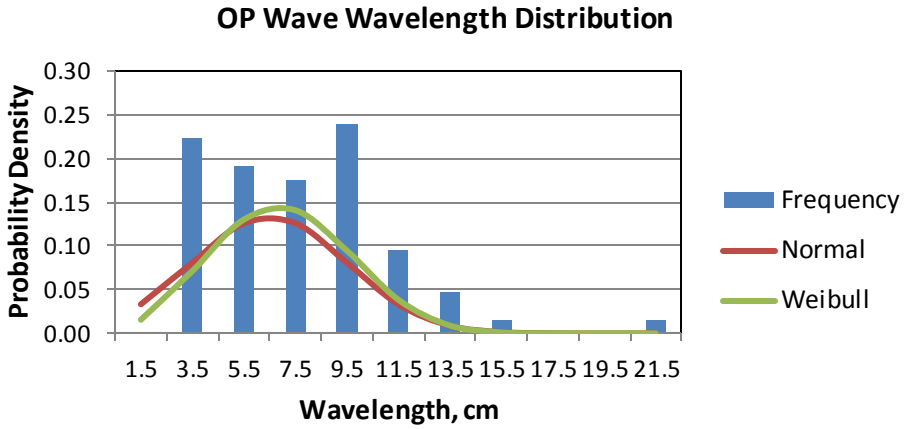

Figure 12: OP wavelength distributions.

Similar binning procedures where applied to amplitude and wavelength data for both wave types. The distributions of this data are displayed in Figure 46 through Figure 49. In general, the skewed populations with extremal ends lead to a better fit with a Weibull distribution. The data on both IP and OP waves can be summarized in Table 1 below.

Table 1: Wave data summary.

OP Waves	Amplitude (cm)	Wavelength (cm)	Fiber Angle (deg)
Min	0.02	1.58	0.59
Max	0.85	21.49	39.01
Mean	0.17	6.74	8.55
Standard Deviation	0.11	3.00	2.82
IP Waves	**Amplitude (cm)**	**Wavelength (cm)**	**Fiber Angle (deg)**
Min	0.11	1.08	8.68
Max	1.18	28.12	50.66
Mean	0.37	4.75	26.73
Standard Deviation	0.23	4.96	9.26

A summary of the adhesive bond parameter data collected is shown in Table 2 and Table 3 below. Plots of the data can be found in the Appendix; Figure 50 through Figure 52.

Table 2: Summary of spar case parameters.

Spar	Thickness (cm)	Void Width (cm)	Void Height (cm)	Porosity (%)
Average	1.42	0.83	0.45	1.48
Min	0.70	0.22	0.13	0.71
Max	3.05	3.12	0.89	2.57

Table 3: Summary of mold line case parameters.

Mold Line	Height (cm)	Base (cm)	Void Width (cm)	Void Height (cm)	# of Plies	Ply Drop Length (cm)	Ply Drop Height (cm)	Aspect Ratio (L/H)
Average	1.91	6.32	0.28	0.27	16.00	3.48	1.82	1.91
Min	1.43	2.63	0.12	0.18	12.00	2.16	1.13	1.73
Max	2.73	10.30	0.54	0.37	20.00	4.34	2.28	2.31

B. Discussion of Test Specimen

i. Design of Test Coupons

Three waveforms for each type of flaw were systematically chosen for testing based on geometry characterization and statistical significance (Table 4, As-Built). For the case of the OP waves, waves OP1 & OP2A were chosen because their angles are almost identical, however, they did have statistically significant and varying amplitudes & wavelengths between them. The particular angle chosen was done so to yield two data points around the angular region of interest (data from a failed blade section). The third OP wave chosen (OP4A) has essentially mean values for all three parameters. Thus, it lands in the middle of all of the parameter distributions. This provides an excellent data point for describing an OP wave common to the specific wind turbine application. By design, it also delivers baselines values for which to compare the effects of amplitude and wavelength independently with the OP1 and OP2A results. Similar to the OP test wave designations, IP test waves IP2 and IP 3 were chosen such that the angles are almost identical. Moreover these values for off axis fiber angles are in the outer regions of the angle distributions. IP1 also utilizes mean values for all of the parameters.

The first round of mechanical testing was on coupon size specimens. Final validation may require larger scale testing.[5] Preliminary consideration was given to scaling coupon test specimens to better describe the full scale response of a flawed structure. The majority of literature describing scaling effects of composite materials tends to converge to the conclusion the Weibull approach to size effects and the statistical nature of fracture is valid as a first order treatment.[8-12] In general, Weibull scaling analysis is based on the so-called weakest link theory which states that with increasing material volume, the population of defects increases and therefore the probability of a failure from a flaw becomes more likely. This is expressed mechanically by a lowering of fracture strength with increasing material volume. Assuming the same probability of survival between small and large scale composites, the ratio between fracture strengths can be found with the following expression:

$$\frac{\sigma_1}{\sigma_2} = \left(\frac{V_2}{V_1}\right)^{\frac{1}{m}} \tag{1}$$

where $\sigma_{1,2}$ are the fracture strengths, $V_{1,2}$ are the volumes and m is the Weibull moduli.[13]

Research conducted on unflawed glass/epoxy uni-axial laminate test specimen has shown a typical Weibull modulus of 29.1.[12] It is apparent from this literature investigation that application of results from coupon level testing to full scale projections will need to consider scaling effects. The question then arises of how the flaws found in thick as-built sections should be scaled for introduction into the smaller coupon level specimen at the onset of a testing program. The theory behind the weakest link phenomenon should still be applicable. Therefore it was concluded that the flaws themselves would be scaled volumetrically, by the same volumetric ratio between the coupons and as-built sections.

Review of the blade section images showed that OP wave flaws were found in laminates that had an average thickness of 1.1". This is only considering the layup which contained the flaw. Other features which may have contributed to the overall sectional thickness such as gel coats, core material and non-unidirectional plies that caped the flawed uni-axial layers were not considered. The standard deviation of the thickness data set is 0.139 (~10%), therefore one can conclude the average thickness value is adequate. Comparisons were made between the coupons and as-manufacture sections utilizing the same length (coupon gauge length) and unit width. Coupon dimensions as well as static testing procedures and results are described in Ref. 5. The 4-ply laminate test specimen have a thickness of ~0.125", which is 8.78 times smaller (volumetrically) than an actual as built blade sections. Inputting the volume fraction and utilizing a modulus of 29.1 in Eq. (1), the Weibull scaling expression, it was found that the fracture strength for the larger as-built blade sections is expected to be approximately 7.1% less than the coupons.

In order to scale the as-built flaw waveforms, the mathematical description of each wave was integrated over the half wavelength to calculate the cross-sectional area of under each OP flaw curve. This is the only parameter needed as unit width was considered. The volumetric ratio between the full scale blade sections and our test specimen was then applied to the as-built flaw cross sectional area. Knowing the scaled cross sectional area, the amplitude and wavelength of each wave was solved for. This analysis is appropriate for the OP waves only. The IP waves, as the name suggest, are planar and need not consider volume. Therefore they were all scaled by the same ratio in order to fit within the coupon dimensions. The scaled wave forms are shown in Table 4. It was the scaled waves that were built into the coupons for Round 1 testing. Additionally the amplitude and wavelength match up with IP3 and IP2 respectively allowing for analysis of those parameters independently.

Table 4: Scaled wave form designations for testing.

OP Wave 1, mm	As-Built	Scaled	IP Wave 1, mm	As-Built	Scaled
Max Amplitude	8.5	2.9	Mean Amplitude	3.7	1.85
Mean Wave Length	67.4	22.8	Mean Wave Length	47.5	23.75
Angle, deg	34.9	36.8	Angle , deg	24.8	24.8
OP Wave 2A, mm	**As-Built**	**Scaled**	**IP Wave 2, mm**	**As-Built**	**Scaled**
Mean Amplitude	1.9	0.7	99% Amplitude	9	4.5
Min Wavelength	15.8	5.4	Mean Wavelength	47.5	23.75
Angle, deg	34.99	34.8	Angle, deg	48.9	48.9
OP Wave 4, mm	**As-Built**	**Scaled**	**IP Wave 3, mm**	**As-Built**	**Scaled**
Mean Amplitude	1.9	0.7	Mean Amplitude	3.7	1.85
Mean Wave Length	67.4	22.8	10% Wave Length	20	10
Angle, deg	9.7	9.4	Angle, deg	47.8	47.8

Vacuum Assisted Resin Transfer Molding (VARTM) is a typical blade manufacturing process and was chosen for the manufacture of test specimen in this investigation.[14] The mostly uni-directional PPG-Devold 1250 gsm areal weight E-glass was used with a Hexion RIM 135 resin system, as these materials closely resemble materials found in production blades. Variations in the process were made to introduce

the three flaw types; IP waves, OP waves and porosity. For the case of IP waves, stitching in the glass fiber mats was first removed in the section which was to contain the flaw. The fiber was then manipulated by hand and secured in place to introduce the waves. OP waves were built by first casting a solid resin stick in a mold with machined sinusoidal grooves. The fiber mats were then placed over the cured resin sticks. For porosity, cavitation bubbles were introduced in the resin mixing process. The aerated resin was then shot through the plate. The porosity content was not known during manufacture.[5]

ii. Use of Inspection Techniques to Characterize Defects in Test Specimen

Manufacturing defects as well as in-service damage can be hard to detect in composite structures, particularly if the flaw is subsurface. Destructive inspection procedures have their use in laboratory and forensics studies. However as the name suggests, the part is no longer useable after the inspection procedure. Therefore the use of non-destructive evaluation (NDE) is growing throughout the industry. There are several NDE techniques used in detecting defects in composite structures. The most commonly used techniques are visual, audio sonic (coin tapping), radiography, ultrasonics, and mechanical impedance testing.[15,16] The BRC is engaged in evaluating these and other technologies such shearography and thermography for their applicability to wind turbine blades. One technology that can be extremely useful in the laboratory is Computed Tomography (CT) scanning. Unfortunately, CT scanning is not feasible for extremely large scale objects such as whole wind turbine blades.

Computed Tomography (CT) was found to provide the most amount of accurate information on flawed composites. Three dimensional renderings of specimen allow for precise measurement of the actual flaw geometry introduced into the coupons. A medical imaging CT scanner (Figure 13) was used successfully on randomly selected samples of the test specimen used in this investigation. It is of critical importance to have accurate measurements of the introduced flaws in developing analytical/empirical damage correlations.

Figure 13: CT scanner.

Figure 14: Coupon with IP wave highlighted.

Figure 14 shows an example of a coupon with a manufactured IP flaw. This wave can be measured on the surface but there is no guarantee that the subsurface layers contain a flaw with the same geometry. In this particular case, they did not. Figure 15 shows through thickness layer by layer radiographs which clearly indicate that there are two different wave forms within the four different laminate layers. The waves were easily measured with the software interface. The same process can be utilized to measure OP waves.

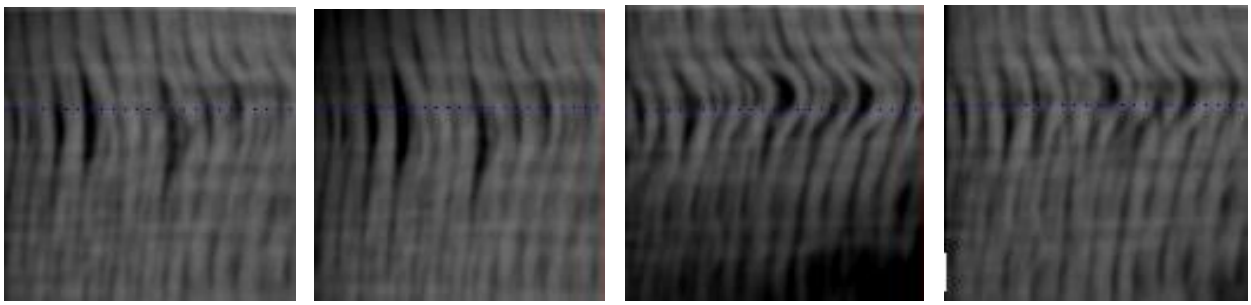

Figure 15: IP wave layer-by-layer radiograph

The results from post processing of the non-tested coupons showed strong variations between the plies of each laminate. In order to rectify these discrepancies, a coupon is characterized by averaging the individual ply laminate values. When the characterized coupons are compared, strong variations exist between the coupons as well (Figure 16 and Figure 17). These results indicate that all test specimens should have their flaws characterized prior to testing for establishing benchmark effects of defects data.

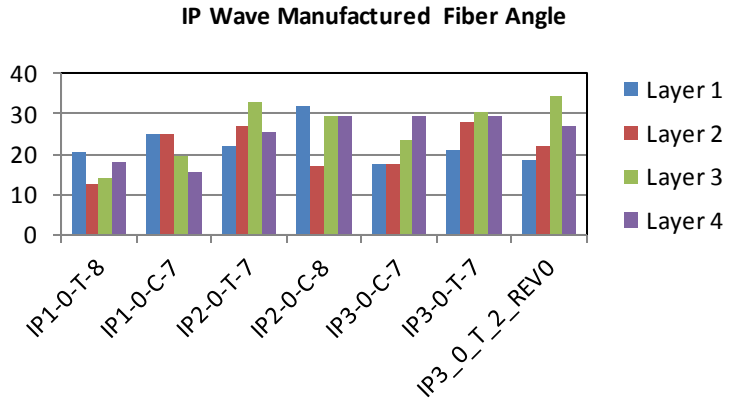

Figure 16: Variations of fiber angle within and individual coupon

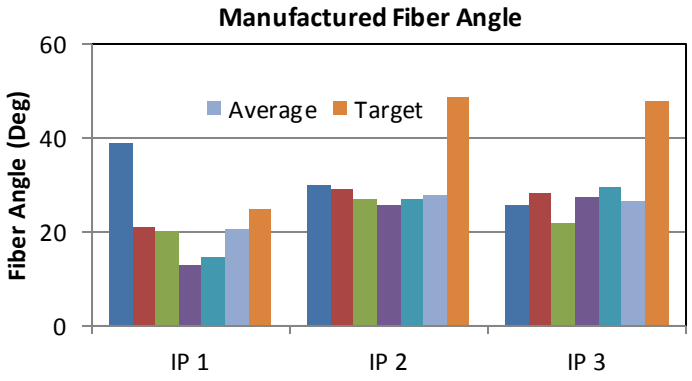

Figure 17: Variation of fiber angle between coupons

Characterization of porosity content in composites materials is particularly troublesome in large parts. It is not uncommon for wind turbine blade manufactures to be unsure of the porosity content in their

blades[*]. Even at the laboratory scale, evaluation of porosity content is labor intensive and time consuming. The method employed by the MSUCG with the most success is microscopy. For this process specimen are cut into small pieces, mounted in acrylic resin and then polished. Depending on the size of the voids either an optical or Scanning Electron Microscope (SEM) is used to take digital images of the cut surface plane. Image processing techniques are then used to identify the location and size of gas inclusions. From this data a planar area fraction of porosity content is established. This value is then extrapolated to percent porosity by volume. An image taken by a scanning electron microscope on a specimen with induced porosity is shown in Figure 18.

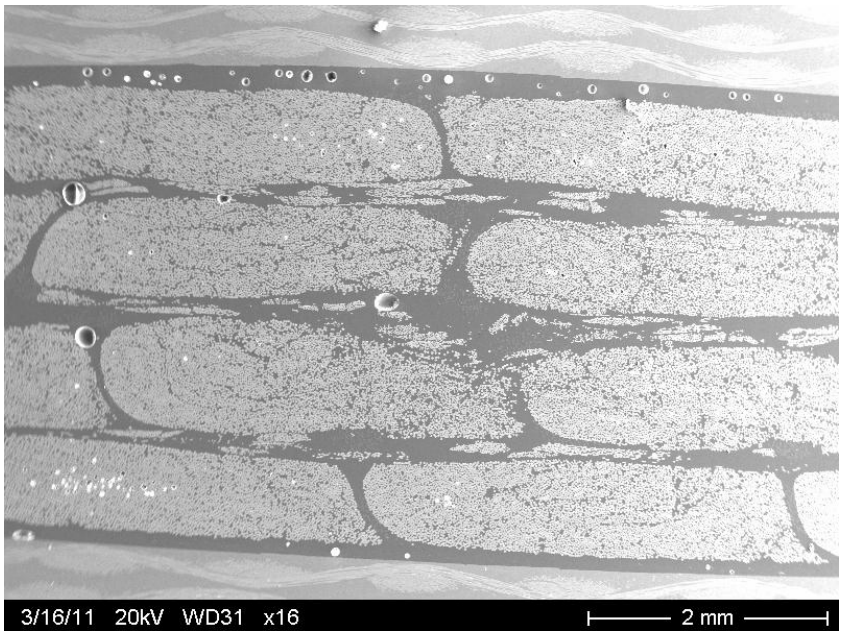

Figure 18: SEM Image of a porosity test specimen.

Presently a method for establishing porosity content of test specimen using the CT scanner is under investigation. The Hounsfield Scale is a quantitative scale for describing radiodensity, or more precisely the linear attenuation of x-rays through a material. By definition, distilled water and air at standard atmospheric pressure and temperature have values of 0 and -1000 Hounsfield Units (HU) respectfully.[17] The CT scanner can measure the attenuation of the scanned material and calculate the radiodensity in relationship to air and water using the following equation:

$$HU = \frac{\mu_x - \mu_{water}}{\mu_{water} - \mu_{air}} \times 1000 \tag{2}$$

where μ_x, μ_{water} and μ_{air} are the linear attenuation coefficients for the material under inspection, distilled water and air respectively.

Figure 19 shows side by side images of porosity and control specimens. It is obvious here that porosity content is no easier to quantify by reviewing a radiograph than it is by using the naked eye. However the images have substantially different radiodensity values. The red square indicates the area over which the radiodensity is averaged. The thickness of the calculation is established on another screen. In this case, the porosity sample has a radiodensity value of ~990HU and the control, a value of

[*] Personal correspondence with wind turbine blade manufacturer.

~1200HU. Initial results from microscopy estimate the porosity content for these test samples at ~1.8%. Further investigations need to be conduct to correlate the two results.

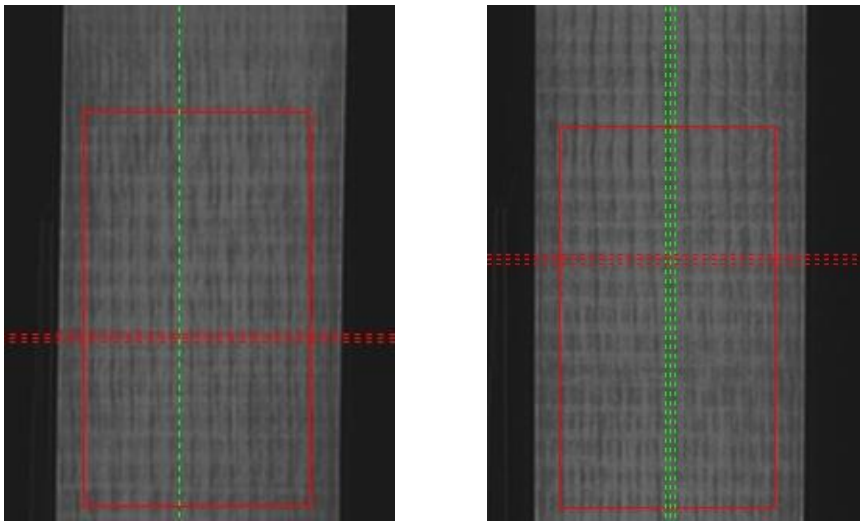

Figure 19: Radiographs of a porosity (left) and a control (right) specimen.

C. Applications in Reliability for Wind Turbine Blades

i. Development of a Probabilistic Reliability Protocol

A framework for a defect risk management and composite structure reliability has been developed. A conceptual flow diagram of this protocol is shown in Figure 20. The protocol consists of four major areas:

- **Effects of Defects**: Flaw and failure data are collected in the field. Testing is performed on specimen with representative defects to generated mechanical properties of flawed laminates. A damage progression model is developed to assess the onset and evolution of damage.
- **Criticality Assessment:** Data from flawed, as-built structures are characterized to describe the defect. This information is fed to the probabilistic evaluation metric and a macro-structure aero-elastic model. Information is imported from the probabilistic model to the criticality analysis. Then the criticality of the defect can be evaluated and a decision is made to operate the structure as is, repair or scrap.
- **Probabilistic Evaluation:** With information on the as-built defect, statistics on flaw distributions and the probability of defect detection, an uncertainty analysis can be performed. From this analysis a limit state function which relates to the structure design criteria can be developed. Random variables are then applied and the probability of failure is discerned. This information is the delivered to the criticality analysis and design process.
- **In-Field Evaluation**: Once the structure has been placed in operation a health monitoring procedure should be implemented. Results from inspections as to the accuracy of the models previously described are then fed back into the design and evaluation procedures.

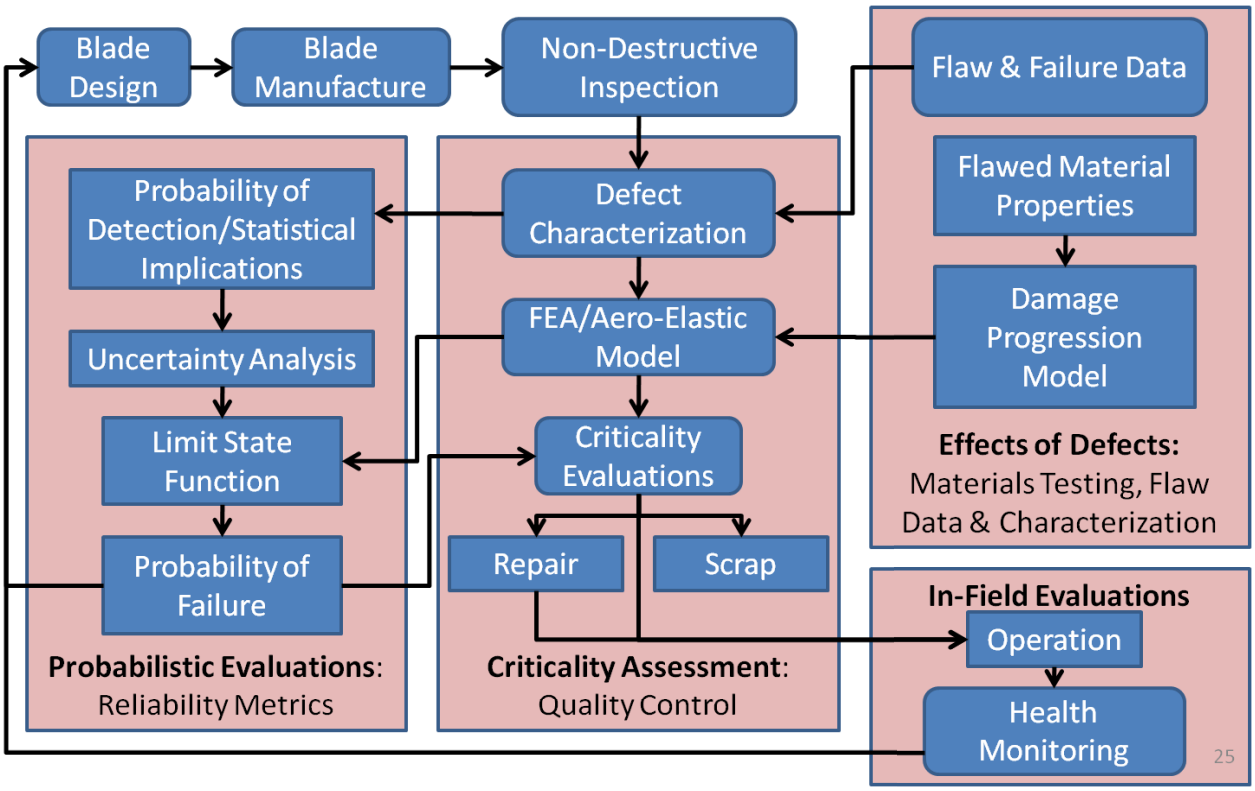

Figure 20: Framework for composite structure defect management and improved reliability

ii. Evaluation of Flaw Criticality

Failure Modes & Effects Criticality Analysis (FMECA) was developed by the U.S. military and NASA to evaluate risks to mission success and improve the reliability of mission critical designs.[18,19] The FMECA has been adopted herein and is under modification to better address the issue of reliability for wind turbine blades. There are two general parameters that define a space in which reliability issues area evaluated; criticality and severity. These definitions have been modified for evaluations of wind turbine blades as follows;

> ***Criticality****:* A measure of the propensity for a flaw to cause a failure. Incorporates damage progression, statistical variations, probability of flaw detection and combined effects of known/unknown proximity flaws. (Probabilistic/Numerical)
>
> ***Severity****:* A quantitative designation based on the local mechanical response of specific as-built flaws, developed from user defined inputs such as global blade properties, specific flaw characterization and location parameters. (Deterministic)

Table 5 lists and describes the different parameters that are included in the criticality analysis. Some of these parameters may not be attainable as a third party investigator, but even with a limited amount of information, the analysis can be useful.

Table 5: Criticality and severity parameters.

Characterization Parameter	Impetus	Comments
Frequency of Occurrence	Required for probabilistic modeling and severity designation	Data collected on flaws from industry surveys and field investigations
Type	Required for flaw classification	Data collected for industry surveys and field investigations. Focus currently is on waviness and porosity/voids
Size	Required for flaw classification	Data collected for industry surveys and field investigations. Examples include Length, width, thickness, amplitude, etc.
Operating Time	Damage progresses with time and loading history	Evaluations of imminent failures will require operating time. Also projections can be made for time to failure
Materials	Required for accurate mechanic response quantification	Different materials can have different damage growth criteria
Structural Design Capability	Required for severity designation	Implications to residual strength; numerically modeled and empirically validated
Environmental Influences	The impact of harsh conditions on various flaws needs to be addressed	Examples include response to temperature variations, fluids and UV radiation
Probability of Detection	Required for probabilistic modeling and severity designation	NDE and other test methods have detection limitations which vary based on flaw type, size and laminate schedule
Failure Mode	Required for severity designation	The way in which a failure is observed, describes the way the failure occurs, and its impact on equipment operation
Location of Blade	Blades can be inspected in several different locations	A blade on the manufactures floor is much easier and cheaper to repair than one on an in-service turbine, etc.
Location of Flaw	Required for severity designation	Stress and strain states vary at different locations, flaws will have varying impacts based on locations
Ability to Repair	Variations to flaw type and size will impact the ability to repair	Affects severity designation. Basically a cost benefit analysis must be performed

All of these characteristics can either be evaluated qualitatively or quantitatively for any flawed blade instance. At present the criticality analysis has been developed as a simple and quick tool, autonomous from the probabilistic modeling propose described in the previous section. A simple algorithm for generating the criticality and severity numbers is used to combine the flaw characterization parameters;

$$S = 1-\sigma_f/\sigma_c \quad (3)$$

$$C = 1-P*L \quad (4)$$

where S is the Severity Number, C is the Criticality Number, σ_f is the ultimate strength of the flawed laminate, σ_c is the ultimate strength of the non-flawed laminate, P is the porosity content modifier and L is the flaw location modifier. Values for σ_f, σ_c, and the ultimate strength of a laminate with porosity were found through the use of laboratory testing described in this paper. The location modifier is knockdown factor based on the location of a flaw in a blade. Currently this is a subjective designation. An effort is

underway to develop a quantitative designation from macro scale finite element analysis of a representative wind turbine blade.

Data from experiments described in this paper are being analyzed to correlate the mechanical response of a flawed laminate to the individual geometric parameters. These results will then be used to build damage models which consider the constitutive response of a flawed composite material.[5] While these models will be largely micromechanical in nature, it is also necessary to consider macro and global effects. For this end, finite element analysis will be used. Analyses of interest include the response of a blade based on global flaw location, location of the flaw in the laminate schedule and the combined effects of multiple flaws. Results from numerical evaluations of specific as-built flawed structure instances will be included in the criticality assessment. One technique being developed presently to evaluate these effects has been to build a blade model in NuMAD (Numerical Manufacturing And Design), a preprocessor for ANSYS developed by SNL. The material properties of regions of interest can be modified to reflect the modified response of flaws from the test data. Examples of the NuMAD interface and a blade meshed in ANSYS are shown in Figure 21.

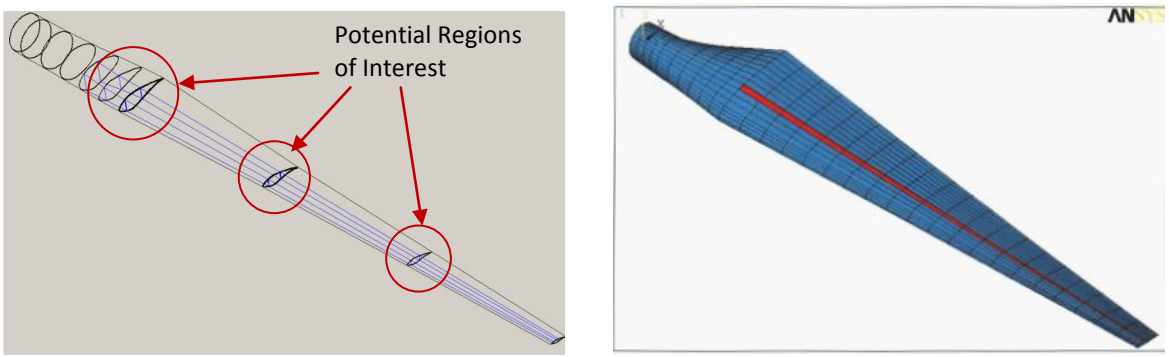

Figure 21: Finite Element Analysis. Blade model building process in NuMAD (left) and a finalized meshed blade model in ANSYS (right)

An example of the current first revision criticality analysis has been performed on a random set of IP waveforms. Input parameter descriptions and mechanical strength correlations can be found in the Appendix. Figure 22 shows the results of this analysis. This is a good example of how criticality and severity are mapped and quadrants are established describing the risk of a specific flawed structure. At present the risk quadrants are place holders. Further analysis and input from manufactures will help define the quadrant space. However, this approach provides a framework for capturing and quantifying manufacturing flaw data from a variety of sources. A tool like this can be employed at the manufactures floor, enabling a quantitative quality control protocol that describes the risk of field failure for a flawed blade. The decision can then be made as to whether or not a blade should be deployed as is, repaired or possibly scrapped altogether. A similar evaluation can be performed on site at the wind farm by installation or maintenance personnel. These investigations may include damage due to transportation or service, as well as manufacturing flaws.

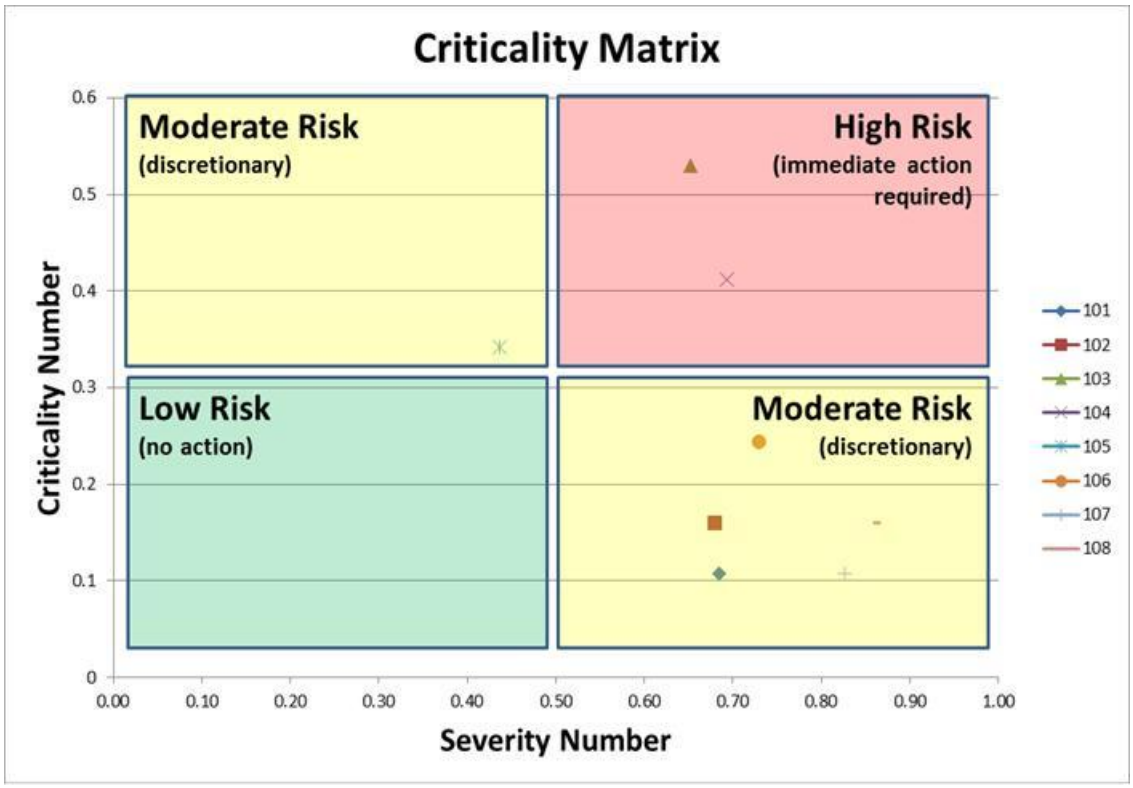

Figure 22: Graphical criticality matrix with defect examples.

D. Flaw Characterization Conclusions

In conclusion, the work presented here has established that characterization of defects common to wind turbine blades is possible. A consistent framework has been established and validated for quantitative categorization and analysis of flaws. However, it relies on accurate and multiple source data collection, with consistent scientific procedures. Preliminary statistics have been reported which show that flaws generally occur with frequencies predominantly describable by the two-factor Weibull distribution. With proper characterization, it is possible to establish the structural implication of a flaw. Results of this investigation are based on a relatively small data set. Efforts will continue in the future to establish partner relationships which will allow for the continued collection of as-built flaw data. Applying the characterization techniques described herein to incoming data will enable the generation of a statistically significant and comprehensive flaw database. It is the goal of this investigation that these tools and data, once disseminated to industry, will contributed to improvements in the reliability of wind turbines. While data has been collected on wind turbines, the framework for analysis and protocols described herein are applicable to the evaluation of any composite structure where preventing failures is critical to safety, performance or economic considerations.

III. Effects of Defects: Initial Testing and Modeling Analysis

The Effects of Defects task is charged with establishing the necessary damage growth and validation tools of composite wind blades to contribute toward a reliability infrastructure for the wind industry. The goal of the initial round of testing was to characterize the mechanical properties of the critical defect types and the results are presented herein. These results were later utilized to build simple analytical models with the purpose of performing laminate analysis with included defects. These models were built with the material properties and convergence was achieved with the damage progression.

A. Effects of Defects Background

Three composite material defect types (Figure 23) were investigated after being deemed critical to blade function and life cycle: IP and OP waviness, and porosity.[20] Extensive studies have reported on the testing of each of the defect types in relatively thin laminates utilizing varying advanced composite materials.[22-34] Much less research related to these and other structural details has been performed for wind turbine blade materials.[33-37] In addition, significant research has been performed modeling flawed composites utilizing different damage progression models.[41-43] It must be noted that much of this research has been performed for industries utilizing smaller scale manufacturing where expense is less critical. Most of this prior research offers a preliminary basis for this work, but it is known that acceptable defects often included in wind turbine blades far exceed what would be acceptable in other industries, such as aerospace. Thus, research specific to understand and model the criticality of defects common to blades is necessary.

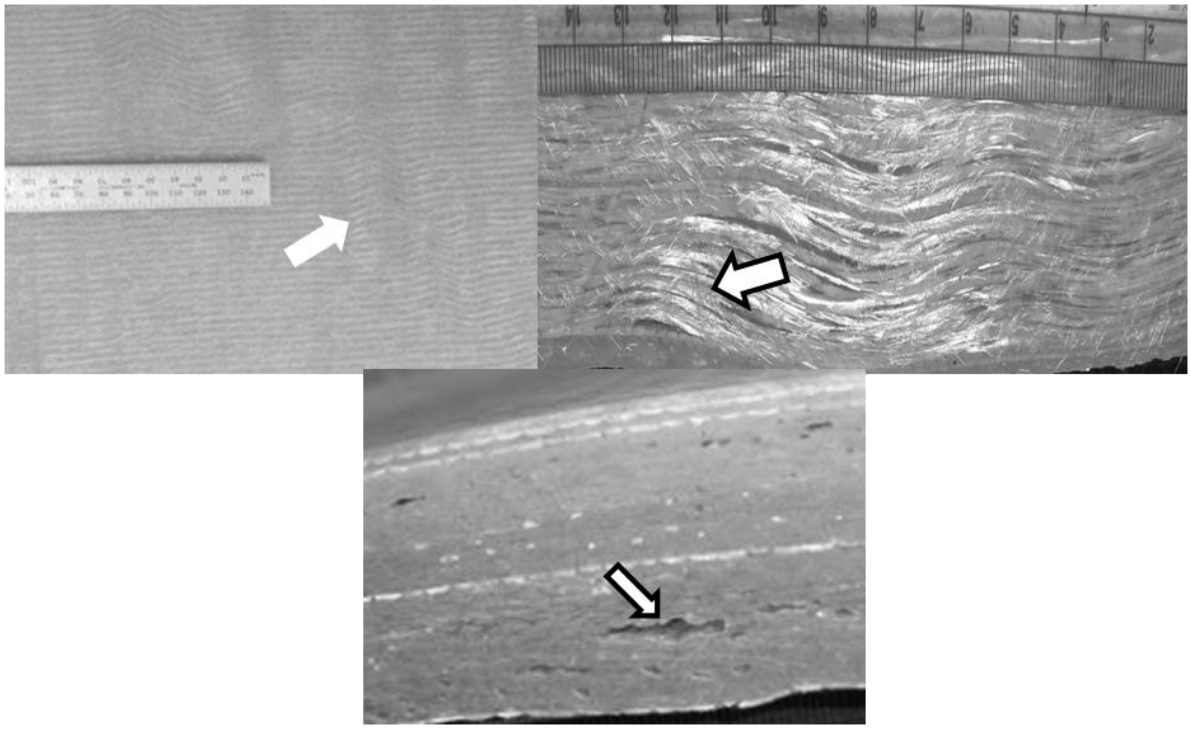

Figure 23: IP waves seen on the surface (top-left), OP waves seen through the thickness (top-right), and Porosity/Voids seen within the laminate (bottom).

Significant research has been performed to understand the effects of porosity on mechanical properties.[22-29] Judd and Wright provide an appraisal of research performed and methods utilized to detect porosity in composite laminates.[22] Findings outlined indicate that mechanical properties degrade significantly (up to 7% decrease in strength) with as little as 1% porosity by volume and in most cases

studies only investigated up to 5-12% porosity by volume. However, effects of voids on mechanical properties has been found to be influenced by void shape, location and size causing a difference in results within test groups of similar void content by volume.[23-25] Furthermore, manufacturing composite laminates with a previously specified amount of porosity is extremely difficult and inclusion of specific size, and shape voids is near impossible. Thus, void content was controlled as much as possible with measurement of these parameters after laminate manufacture. As exact values of the amount of porosity commonly included in wind turbine blades is unknown, it is assumed to be in the 5-20% range based on information given to the BRC.

Fiber waviness studies have most commonly investigated the effects of waviness on compressive strength of OP waves. In general, OP fiber waviness has been found to decrease static compressive strength. Adams and Bell investigated OP waves isolated within a thermoplastic[†] laminate and determined that compressive strength decreased approximately 35% when more than 33% of 0° layers contained waves.[30] Previous research by Adams and Hyer also determined that static compressive strength decreased up to 36% with sudden, catastrophic brooming failures near the waves.[31] Related research has been performed by Mandell and Samborsky, where a through-the-thickness stitching was found to significantly reduce static compressive strength, while static tensile strength had little decrease.[33,37]

Wang determined that static compressive strength reductions increased as the wave severity and percentage of layers with waves in the laminate increased.[34] Failures were noted to be at the maximum fiber orientation. Further, IP waves were found to have a significant reduction in static tensile strength, decreasing further as wave severity increased. Tensile failures were characterized to be delaminations and fiber fractures. In both compressive and tensile cases, wave severity was characterized by aspect ratio (A/λ).

Aided by computational improvements in recent decades, significant progress has been made in many avenues of modeling composite materials utilizing damage progression. Utilizing a simple material property degradation model, Chang and Chang presented a progressive damage model for laminated composites with a circular hole in tension.[42] Convergence between stress and failure analyses were performed utilizing classical lamination theory considering material nonlinearity and property degradation resulting from damage, respectively. Nonlinear finite element analysis was performed and agreement was found between the analytical and experimental data. In the stress analysis, the equilibrium equation and stress-strain relations were derived. The equilibrium equation took into account that once the laminate was damaged a redistribution of the stresses and strains resulted in degraded material properties. Thus, the equilibrium equation was solved at each step utilizing a Newton-Raphson iteration scheme. The failure criteria were defined based on the failure mechanisms resulting from damage: matrix cracking, fiber-matrix shearing and fiber breakage. Based on these criteria, a property reduction model was implemented reducing certain properties to zero upon failure.

Numerical procedures were written based on the following procedural logic:

1. Increase the applied load from P^{n-1} to P^n by a small increment ΔP.
2. Calculate incremental strains Δe_{ij} and incremental stresses $\Delta \sigma_{ij}$ from derived stress-strain relations and equilibrium equations.
3. Update the total stresses σ^n_{ij}.
4. Calculate in-plane stresses in each ply by coordinating transformation.
5. Assess damage using failure criteria equations.
6. Return to the first step if no damage is found or continue to the following steps if damage occurs.

[†] It should be noted that thermoset resins are used exclusively in the wind industry.

7. Stop, if damage has propagated across the laminate and no more load can be added.
a. Continue, otherwise.
8. Update mechanical properties by applying property degradation model.
9. Redistribute stresses and strains in the laminate by applying equilibrium equations again.
10. Return to step (4).

The results were agreement between the analytical and experimental data for seven (7) independent laminates.

Later, Chang and Lessard performed similar work on damage tolerance of laminated composites in compression with a circular hole.[43] A progressive damage model was developed to simulate response from initial loading to final collapse and consisted of stress and failure analyses. Similarly, in the stress analysis an equilibrium equation and stress-strain relations were derived with material and geometric nonlinearities considered. Failure analysis was based on a combination of Hashin criteria and failure criteria developed by Chang in the work above.[42-43] Failure criteria and property degradation models were defined for matrix tensile cracking, matrix compression failure, fiber buckling failure and fiber-matrix shearing failure. A similar logic as above was utilized resulting in agreement between the analytical and experimental data.

Additional research in this area has been performed by others for many different conditions (e.g. material, matrix, loading, fastening, etc.). Eveil (Intl Journal of Mechanics, v2, 2008) developed a 3D failure analysis methodology for composite laminates.[44] This analysis utilizes a similar logic to Chang above with failure criteria based on Hashin and Yeh. Utilization of this advancement to 3D improved error from 25-30% to as low as 2.6%. Tay et al. have compared material property degradation models, element failure method and strain invariant failure theory.[45] Material property degradation is the method used in each of the papers above. The element failure method modifies nodal forces to reflect damage and is employed with micromechanics based failure criteria. It is suggested that these and other alternative approaches may be superior when translating results from specimen level to component and structural levels. Tay et al are not the first to develop these approaches and further research on this end toward a constitutive based model and/or "super element" will be performed as outlined in the future work section below.

B. Round 1: Physical Testing Materials and Methods

i. Materials and Processing

In order to ensure the defects applicability, both the IP and OP waves to be analyzed in this study were based on a survey of wind turbine blades containing these defects.[21] Digital images were analyzed and waves were discretized and mathematically characterized before determining wavelength and amplitude values as shown in above. Statistical analysis of these parameters and scaling were performed to determine the values to be tested outlined in as noted above.

Four layer panels containing each of the defects and defect-free control panels were infused under vacuum with one layer of peel-ply on the top and bottom surfaces and one layer of flow medium on the top surface of the laminate. Mostly uni-directional PPG-Devold 1250 gsm areal weight E-glass was used with a Hexion RIM 135 resin system in all cases. Laminates for each case were manufactured with fiber directions of both 0° and ±45°. The cure profile for each panel was 48 hours at room temperature followed by 8 hours at 80°C. The nominal fiber volume fraction of the panels was 55% with a nominal thickness of 3.2 mm.

The manufacturing process was adapted to include each of the three defect types. Air bubbles were introduced into the resin directly by cavitation during the mixing process prior to infusion. IP waves were introduced by pulling the fibers manually as shown in Figure 24 for a one entire wavelength. OP

wave forms, also for one entire wavelength, were created by casting resin into a CNC machined mold and placing the castings under the laminate as shown also in Figure 24. Wavelengths, amplitudes and estimated fiber misalignment angles are listed in Table II.4 above. Fiber misalignment angles were deemed a more consistent method of wave severity characterization than aspect ratio for this study.[21]

Test coupons were cut from the panels for use in tension and compression testing. Tensile coupons were cut to approximately 50 mm wide by 200 mm long and were tabbed resulting in a gage length of 100 mm. Compression coupons were cut to approximately 25 mm wide by 150 mm with an anticipated gage length of 25 or 38 mm where the wavelengths were greater than 25 mm.

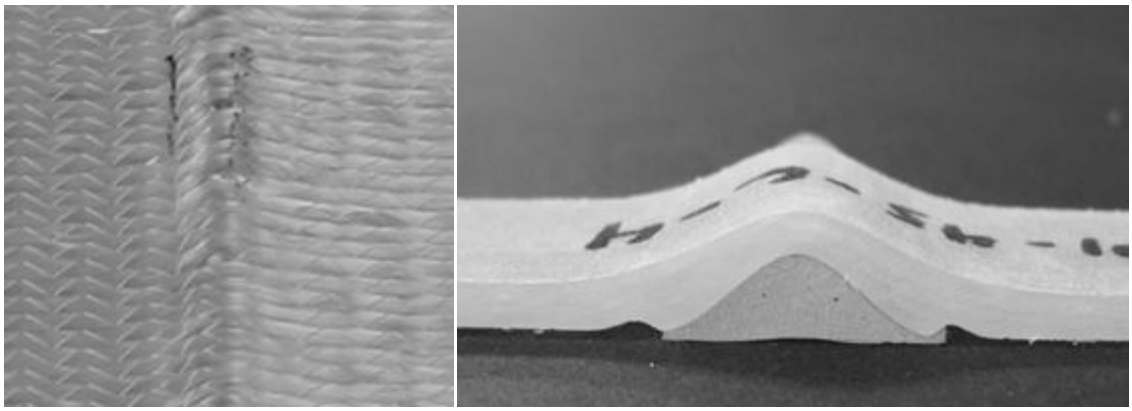

Figure 24: IP waves imparted into a layer in a 0° laminate (left) and an OP wave form used to impart necessary wave into a 0° laminate (right).

ii. Test Methods

The control and porosity samples were symmetrical, while each of the wave samples were not. Test methodology was considered when determining lay-up and coupon dimensions. Coupons were constructed with representative of blade materials and construction processes though scale was reduced. Scaling was required to achieve compatibility with the Instron 8802, 250 kN testing machine and grip capacity (Figure 25). Static ramp tests on the specimens were conducted at a rate of 0.05 and 0.45 mm/s for tension and compression, respectively. A total of approximately 135 coupons were tested with 2-5 in each test group. A digital image correlation system was utilized to measure and analyze the strain field of each specimen type. These displacement data were compared to the displacements recorded from the Instron's LVDT and were utilized where discrepancies were identified. Results of all experiments will be available in the DOE/MSU Composite Material Database.[37]

Figure 25: Representative 0° tensile (left) and ±45° compressive (right) samples being tested.

C. Round 1: Physical Testing Results and Discussion

i. Control

Tensile and compression tests were carried out on control 0° and ±45° laminates with no intentional defects introduced. Stress-strain curves for these tests are shown below in Figure 27 through Figure 29Material properties were calculated as outlined in several ASTM standards that were used a guidelines throughout the this testing and are shown in Table 6 and Table 7.[18-20] The data indicate that the highest strength was observed with the 0° tensile control group with an average of peak stress of 990 MPa while it was approximately 580 MPa for the 0° compressive group. Failures were initiated by matrix cracking followed by ply delamination, load redistribution and ultimately ply failure. Shear stress was approximately the same for both tension and compression at 112 and 124 MPa, respectively, as would be expected based on the observed matrix failures in the ±45° laminates. In addition, a representative sampling of results from the digital image correlation and associated strain fields of the 0° control and several other laminates are shown in Figure 31-Figure 34 below.

ii. Porosity

Specimens containing porosity were analyzed with scanning electron microscope (SEM) to determine the volume of porosity included, which was found to be approximately 1.8% (Figure 26).[1] As noted in Table 6 and Table 7, samples with porosity were shown to have decreases in ultimate stress (84-94%) and strains at failure (82-98%) compared to the control samples. Confirmation of this result may be observed by comparing the control and porosity strain fields (Figure 31 and Figure 32), which indicate lower strains approaching failure. Comparison of these two strain fields also appears to initially indicate that there are more concentrations of higher strain in the porous laminate. Further testing would require this to be determined conclusively.

The exception to the observation of reduced ultimate stress was the ±45° group when tested in compression which was found to be higher in ultimate stress (101%) even though the strain at failure was reduced (91%). Also of interest was the observed increase in estimated modulus of elasticity for this both ±45°groups (103-106%) compared to the control. This could also be a result that shear failure occurs prior to the cracks that are likely to originate and propagate throughout included pores and/or the stiffness is increased due to the resin becoming more brittle with increased porosity. While these initial findings are of interest and appear to agree with previous results where applicable, additional testing at various porosity levels is necessary to determine the critical levels of porosity. It must, however, be noted that these data conclusively states that 1.8% porosity does decrease results in a 6-16% strength decrease and a 2-18% reduction in the strain at failure. This is in agreement with previous research noted above. Further, the decrease in strength and increase in modulus of elasticity for the ±45° compression groups does not appear to differ enough from the control groups to warrant further testing. As with the other groups tested, these ±45° groups tend to fail from edge effects resulting negligible differences in material properties from control groups.

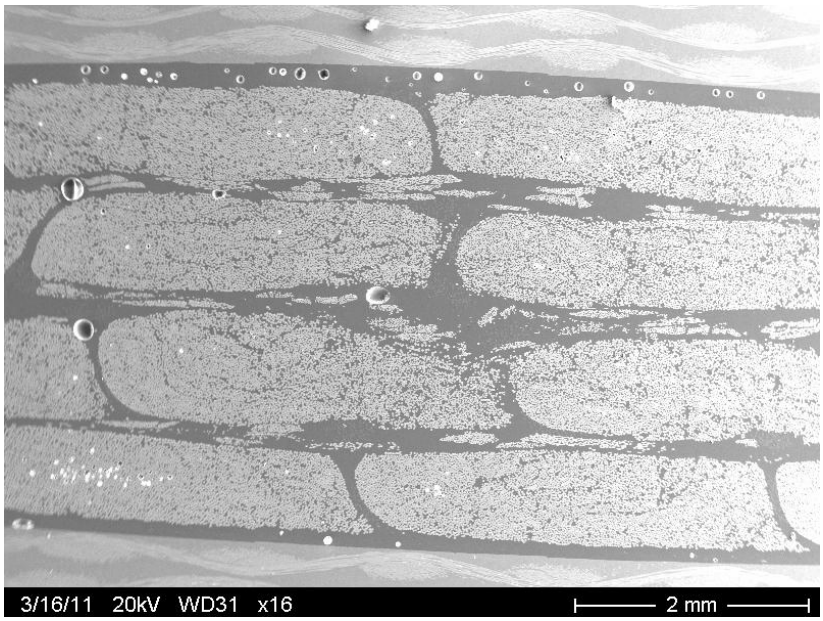

Figure 26: Scanning electron microscopy (SEM) image of porosity sample tested.

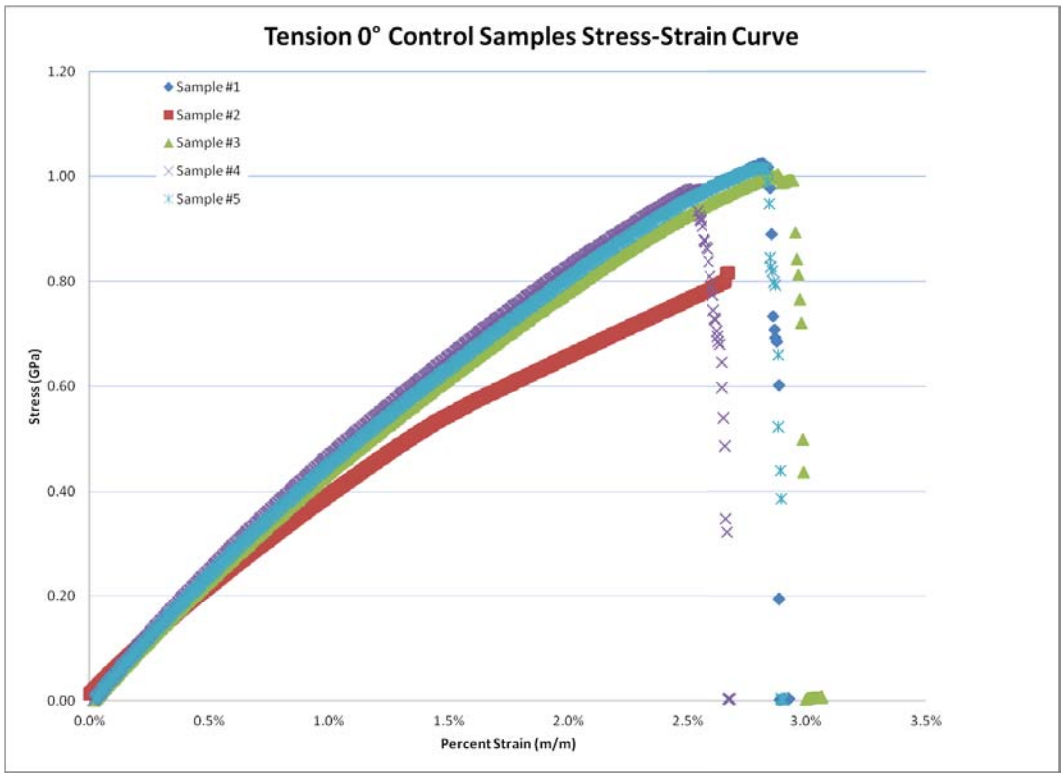

Figure 27: Stress-strain curve for 0° tensile control laminates.

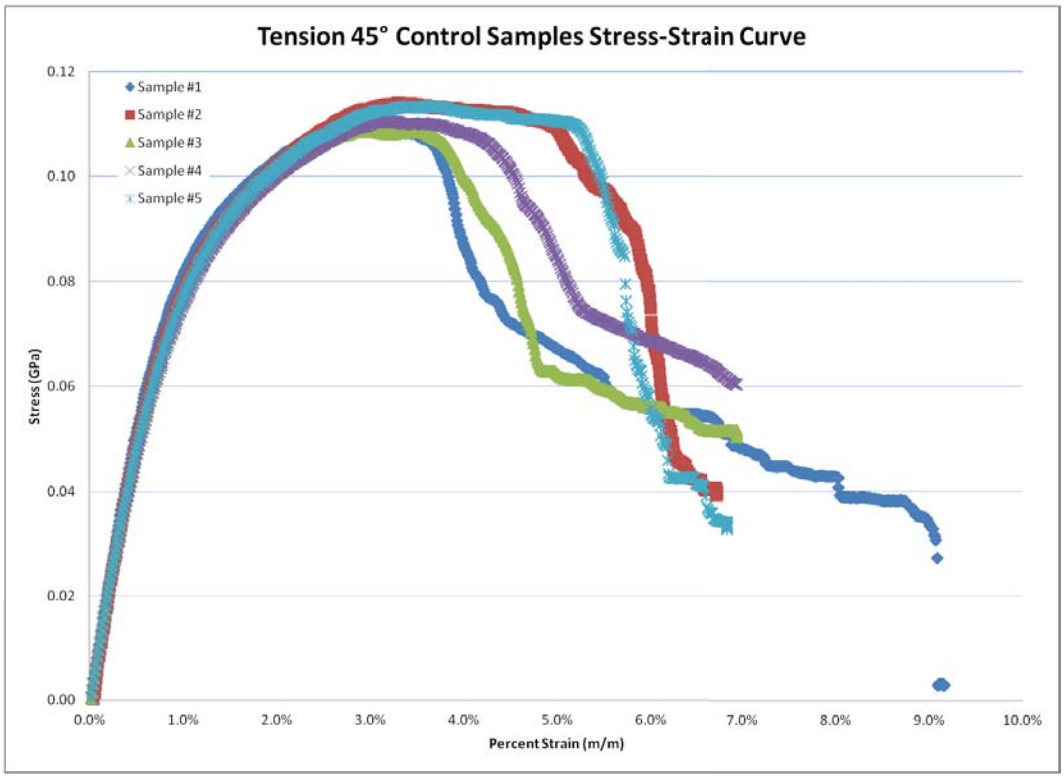

Figure 28: Stress-strain curve for ±45° tensile control laminates.

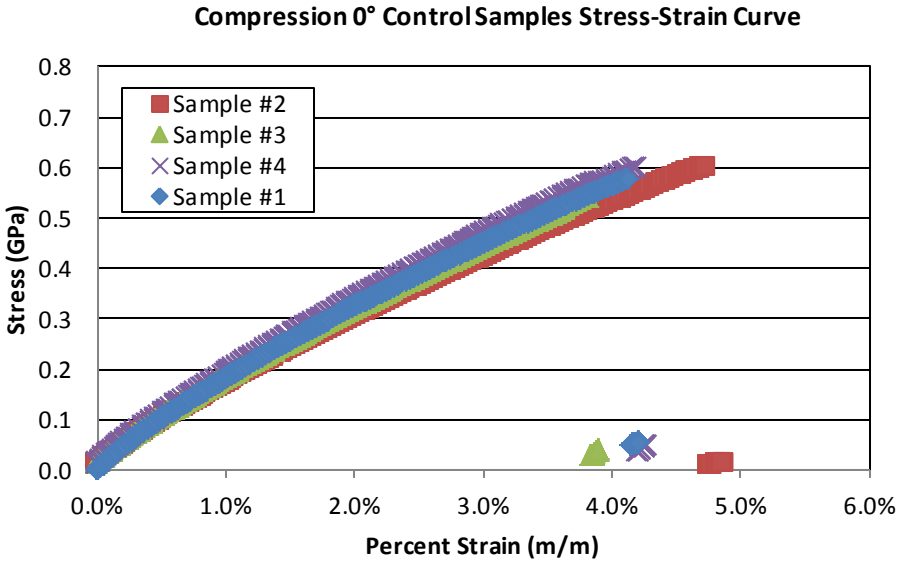

Figure 29: Stress-strain curve for 0° compressive control laminates.

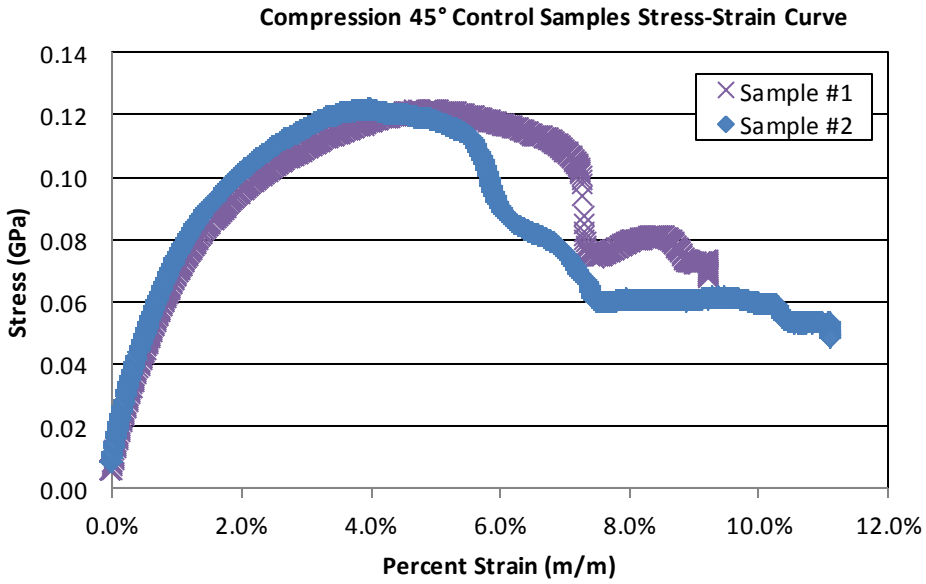

Figure 30: Stress-strain curve for 45° compressive control laminates.

Table 6: Static properties for laminates tested in tension and calculated percentage of control laminates.

Tension	Control		Porosity		IP 1		IP 2		IP 3		OP 1		OP 2A		OP 4A	
	0°	±45°	0°	±45°	0°	±45°	0°	±45°	0°	±45°	0°	±45°	0°	±45°	0°	±45°
Ultimate Stress (MPa)	990	112	950	103	521	108	344	109	226	107	417	84	742	101	752	102
% Control	--	--	96%	93%	53%	97%	35%	98%	23%	96%	42%	75%	75%	91%	76%	91%
Strain at Failure (%)	2.64%	1.44%	2.54%	1.30%	1.66%	1.13%	1.66%	1.72%	1.66%	2.02%	4.77%	4.91%	4.92%	3.06%	4.56%	3.43%
% Control	--	--	96%	90%	63%	78%	63%	119%	63%	140%	181%	341%	186%	213%	173%	238%
Est. Modulus of Elasticity (GPa)	41.1	16.2	39.6	16.6	39.6	18.7	34.8	16.8	24.1	16.6	17.3	5.9	32.1	16.1	31.2	15.3
% Control	--	--	96%	103%	96%	115%	85%	104%	59%	103%	42%	36%	78%	100%	76%	94%
Poisson's ratio	0.27															

Table 7: Static properties for laminates tested in compression and calculated percentage of control laminates.

Compression	Control		Porosity		IP 1		IP 2		IP 3		OP 1		OP 2A		OP 4A	
	0°	±45°	0°	±45°	0°	±45°	0°	±45°	0°	±45°	0°	±45°	0°	±45°	0°	±45°
Ultimate Stress (MPa)	582	124	491	125	257	165	216	181	216	139	95	43	227	90	207	86
% Control	--	--	84%	101%	44%	133%	37%	147%	37%	112%	16%	35%	39%	72%	36%	70%
Strain at Failure (%)	4.22%	4.50%	3.46%	4.10%	2.01%	2.30%	2.02%	1.98%	2.19%	3.19%	1.69%	4.32%	2.50%	3.63%	2.21%	3.25%
% Control	--	--	82%	91%	48%	51%	48%	44%	52%	71%	40%	96%	59%	81%	52%	72%
Est. Modulus of Elasticity (GPa)	18.3	7.2	17.9	7.6	16.9	11.8	15.2	13.3	14.5	9.1	6.1	2.1	11.3	5.8	11.5	5.5
% Control	--	--	98%	106%	92%	164%	83%	185%	79%	127%	33%	29%	62%	80%	63%	77%
Poisson's ratio	0.28		0.18		-0.28		-0.43		-0.21		0.45		-0.02		0.03	

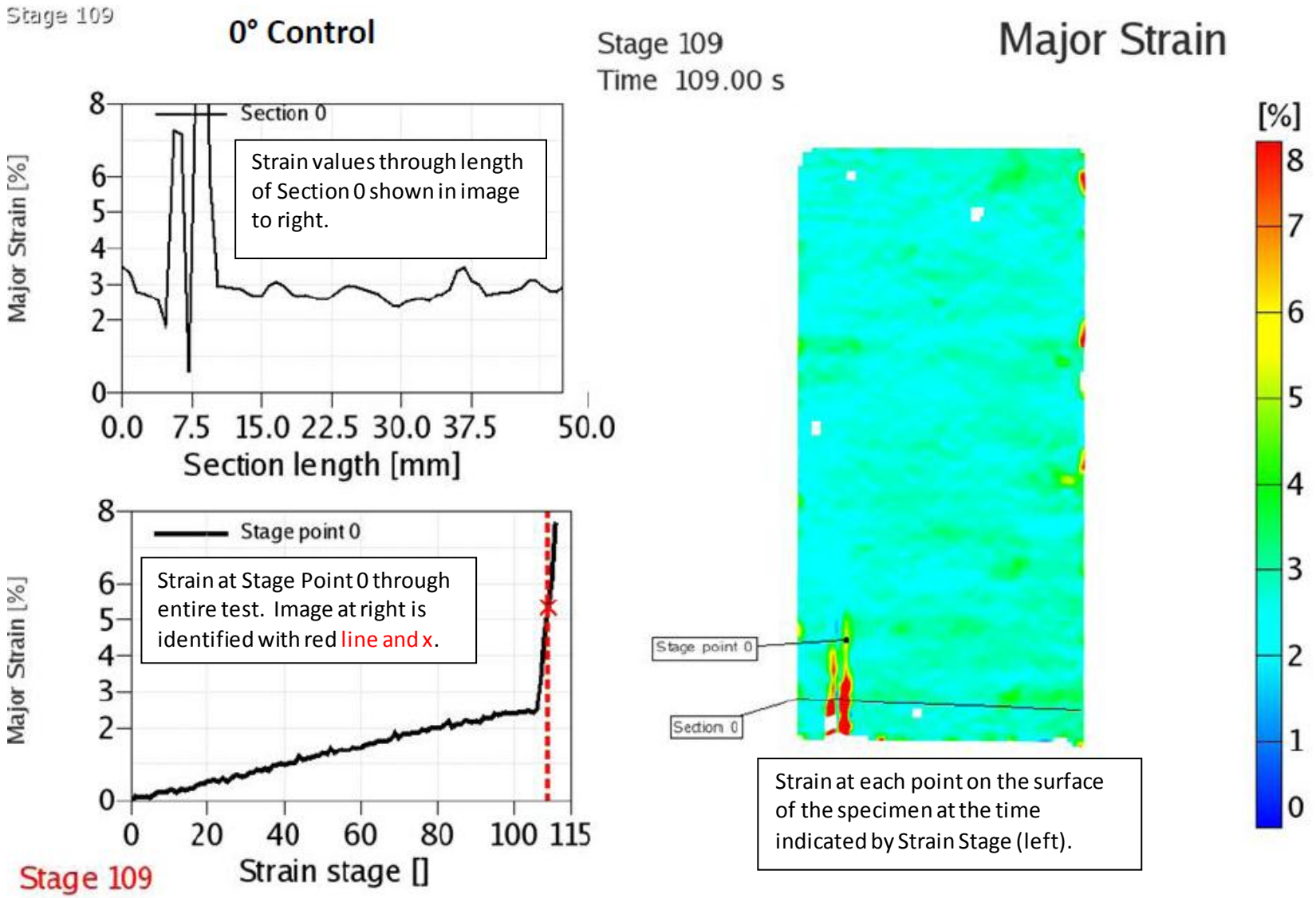

Figure 31: Representative images near failure of 0° control laminate tested in tension from the digital image correlation system.

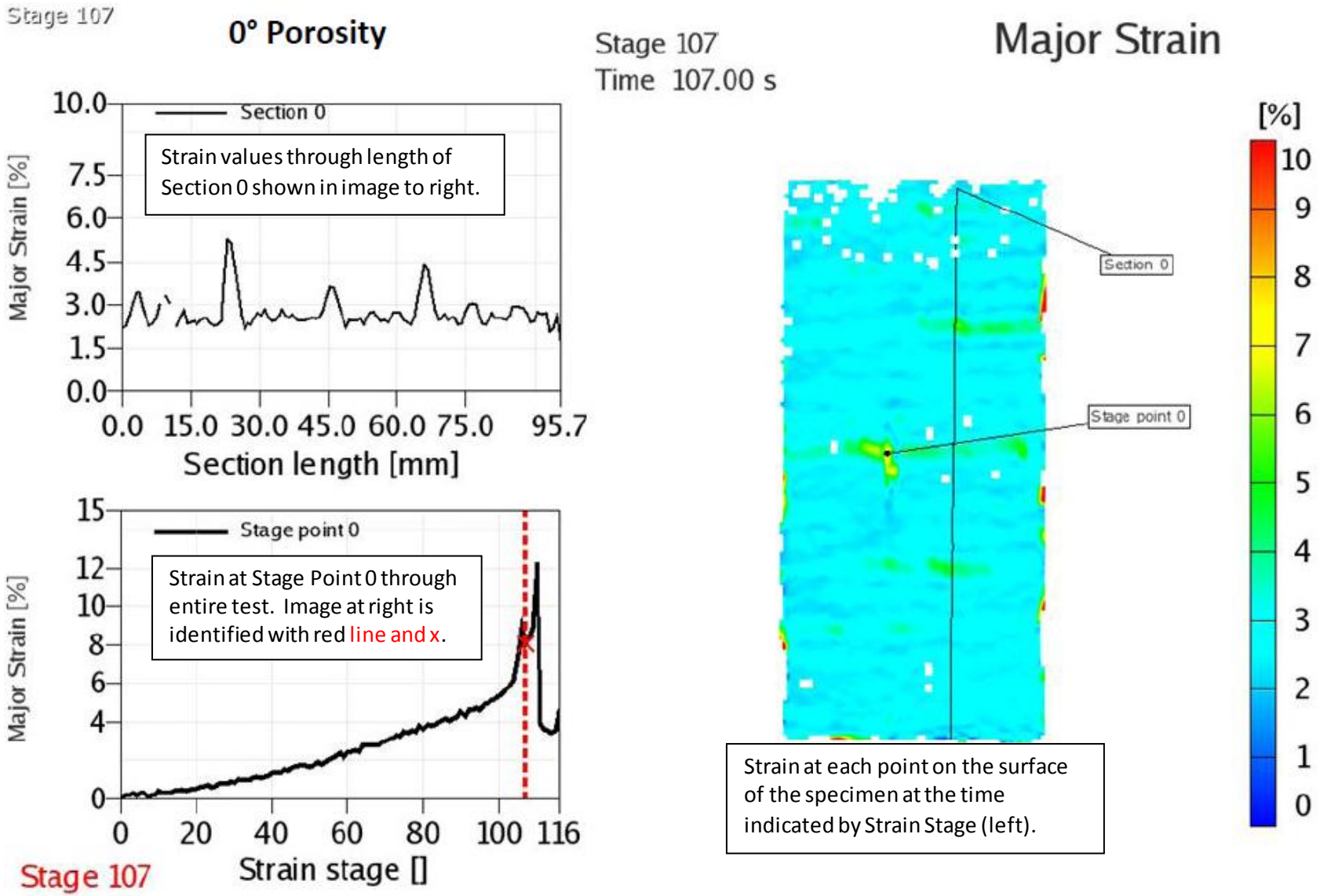

Figure 32: Representative images near failure of 0° porosity laminate tested in tension from the digital image correlation system.

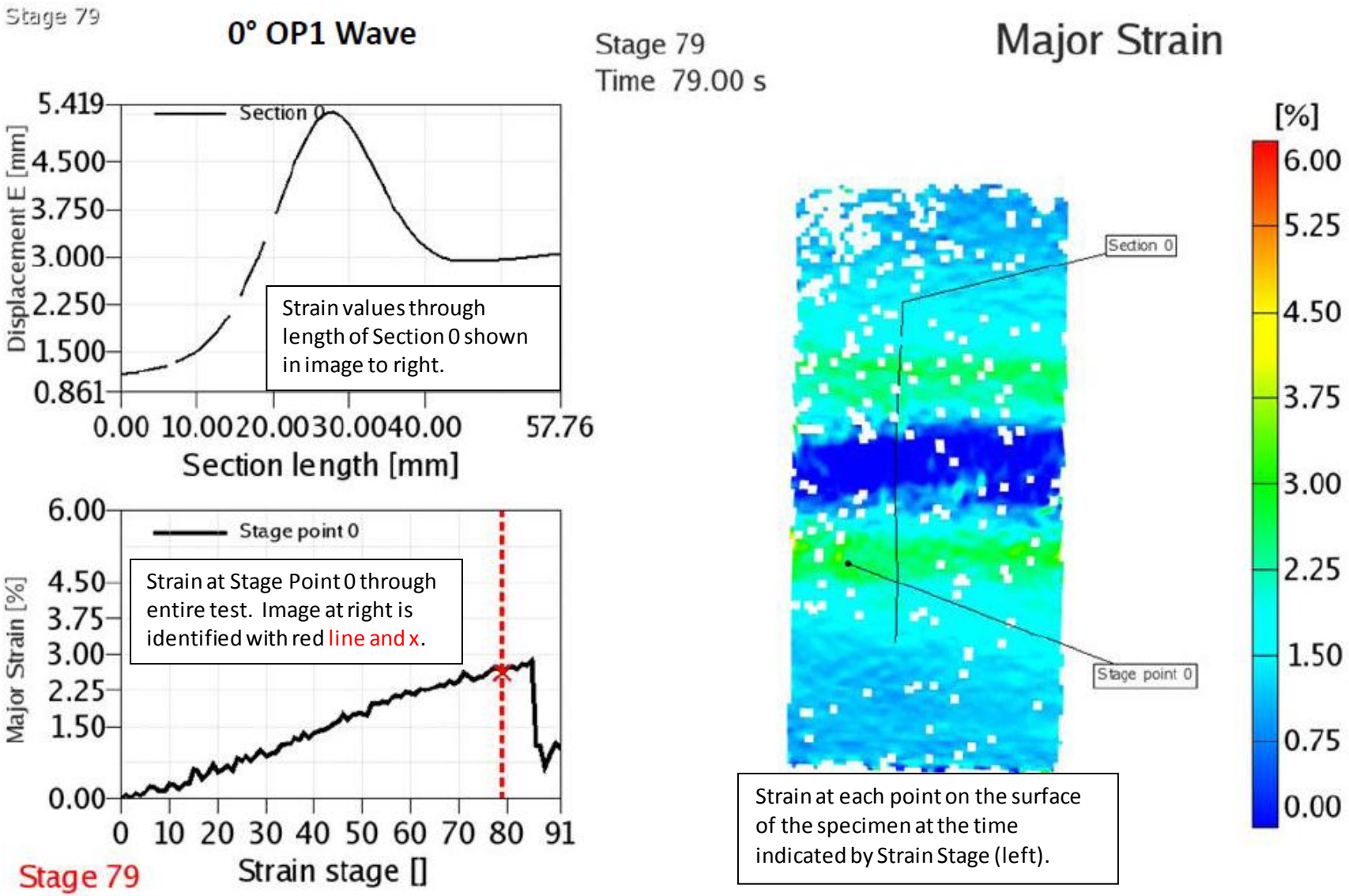

Figure 33: Representative images near failure of 0° OP1 wave laminate tested in tension from the digital image correlation system.

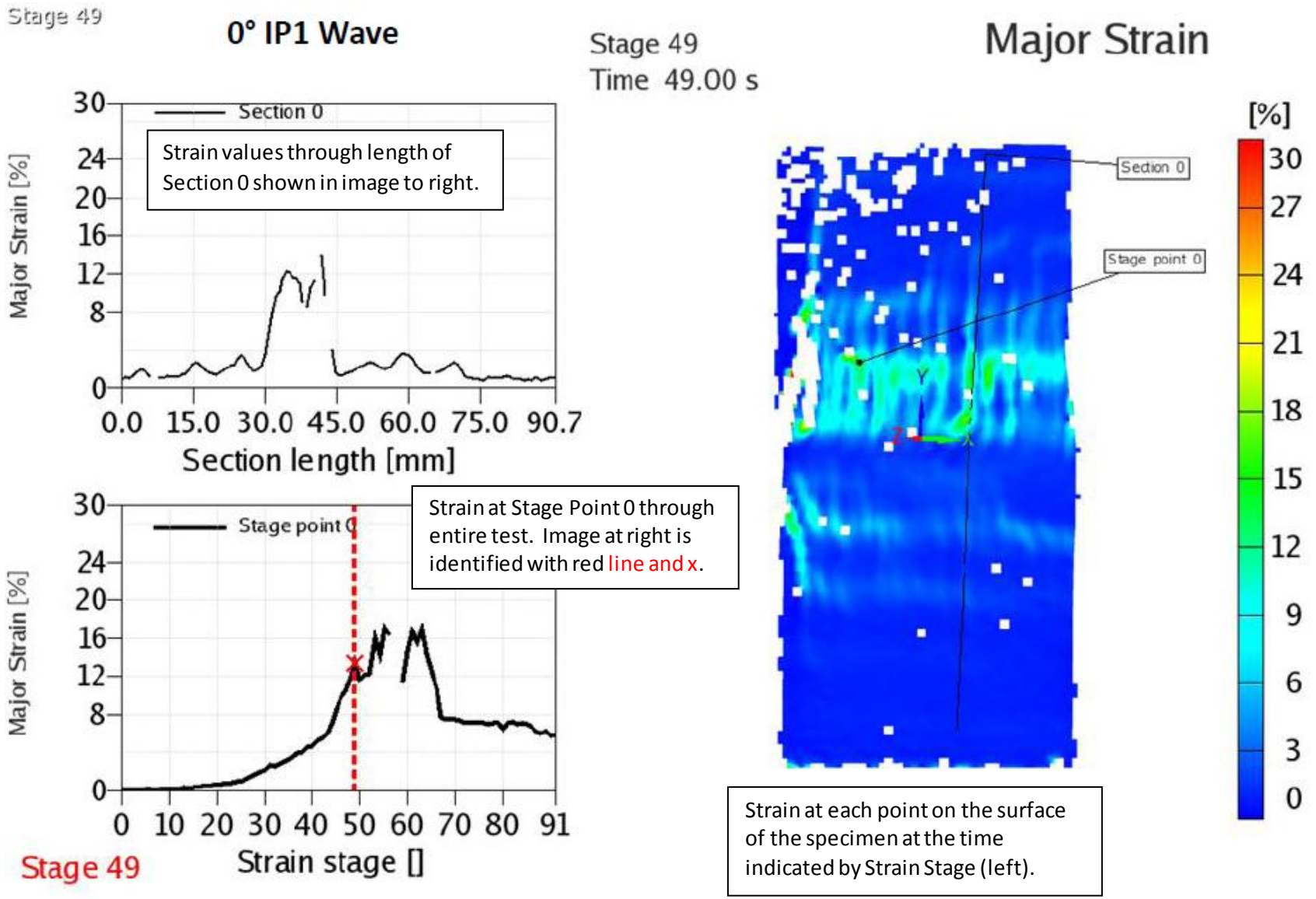

Figure 34: Representative images near failure of 0° IP1 wave laminate tested in tension from the digital image correlation system.

iii. In-Plane Waves

Test results for the IP wave groups are also noted in Table 6 and Table 7. Results from test observation and the digital image correlation suggest that each of the IP wave groups was noted to have similar damage progression. First failures were noted at low loading levels in areas where fibers were not continuous through the length of the sample. As strain levels increased, cracks initiated in the resin at the ends of the wave before delaminating and growing through the entire wave section resulting ultimately in fiber failure (Figure 35). These observations combined with the strains at failure indicate that damage accumulation was lower than the control group.

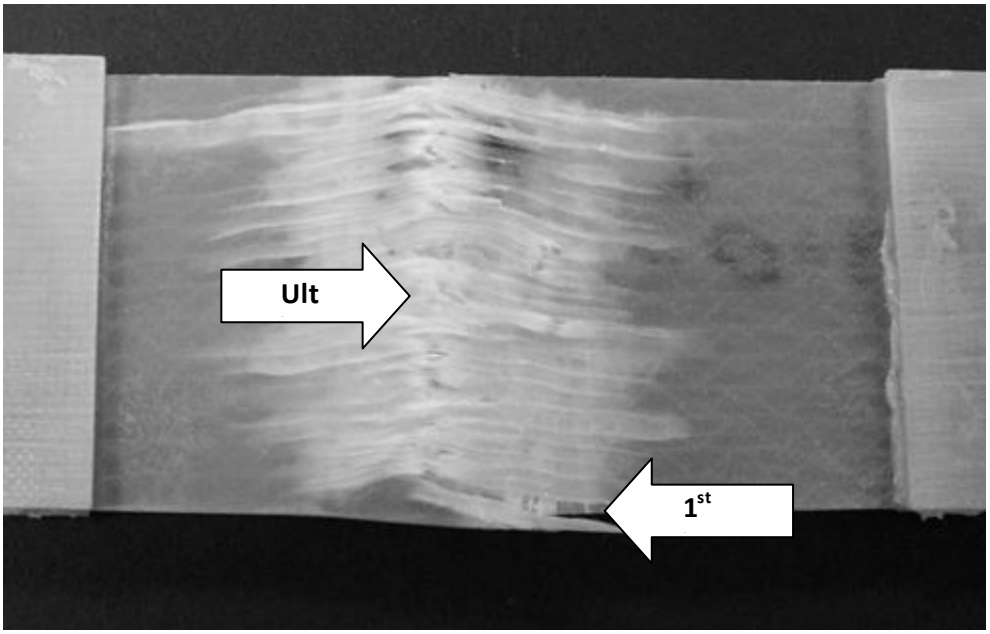

Figure 35: Failed IP tensile specimen showing delamination and fiber failure.

Ultimate stress values for the each of the 0° IP wave groups tested in tension were found to have a significant decrease in ultimate stress; 54% down to 25% of the control for waves IP 1 through IP3, respectively. As noted in Table 4, the amplitude and wavelengths for each these waves varied and even though IP1 had the highest ultimate stress it also had the largest amplitude. Further, IP2 has larger amplitude and wavelength than IP3 while the ultimate stress for each is approximately the same, though IP2 has a larger strain at failure than IP3. Based on previous research, similarity of the results was expected between the IP2 and IP3 groups as the fiber angles were similar between the two groups.

It is also interesting to note that the modulus of elasticity for these groups was 85-106% of the control, indicating that the change in fiber direction increased stiffness. This is likely due to the load matrix "locking" the fibers into place at the ends of each wave before the matrix cracking noted above. Thus, initial stiffness was similar to the control even though the ultimate stresses and strains were notably lower. Very similar results and trends were also noted for the 0° IP wave groups tested in compression. Overall, IP waves resulted in decreased material properties when included in 0° laminates.

The ±45° groups tested in tension had ultimate stress values very similar to the control group (96-98% of control) though the strains at failure were found to be lower (63-94%). Of note was the modulus of elasticity increased compared to the control group (103-116%), likely for the same reasons as the 0° IP groups noted above, which resulted in significantly lower values for Poisson's ratio. The ±45°compression results were rather remarkable as the ultimate stress for all IP wave groups was significantly higher compared to similar control groups (112-133%) even though strains at failure were

lower (44-71%). This resulted in significantly stiffer ±45° laminates causing a negative Poisson's ratio for the IP wave groups in compression. These results are due to the increase load carrying ability of the laminates caused by the fibers in the wave approaching 0°. However, both IP2 and IP3 had the same fiber angle though the ultimate stresses in each was different; 0.18 and 0.14 GPa, respectively. This may be from unexpected responses during manufacture that resulted in differences between initial imparted amplitudes, wavelengths and fiber angles and what was contained in the final laminate. Confirmation is indicated by the variation in the non-destructive testing of these laminates performed in the Flaw Characterization portion above.[1] In short, while properties decreased in 0° laminates including IP waves, laminates including ±45° performed as well or better than control eliminating the need for further analysis. In addition, while further analysis may be helpful for portions of these groups, these data offer excellent convergence points for the forthcoming analytical models.

iv. OP Waves

Test results for the OP wave groups are also noted in Table 6 and Table 7. Results from test observation and the digital image correlation suggest that each of the OP wave groups was noted to have similar damage progression. Also similar to IP waves, as strain levels increased cracks initiated in the resin at the ends of the wave before delaminating. However, unlike the IP waves, after delamination the failure area for the OP wave specimens were concentrated at the peak area of the wave. This was due to the fibers being pulled straight and the center of bending being at the peak of the wave (Figure 36). It must be noted that the wave forms for all of the OP1 groups delaminated during testing. This resulted in an extreme decrease in the ultimate stress and modulus of elasticity results of the OP1 groups in both tension and compression. These results also suggest that partial delamination may have occurred in other groups.

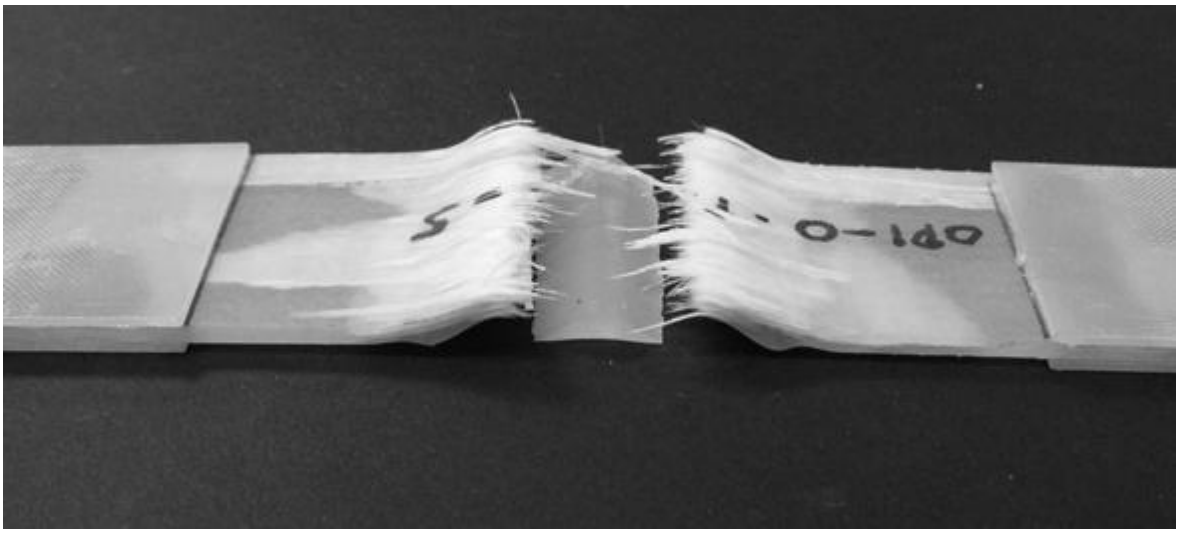

Figure 36: Failed OP tensile specimen showing interlaminar delamination, fiber failure and delaminated resin wave form.

Ultimate stress and strain at failure values for the OP2A and OP4A 0° and ±45° tension groups were decreased compared to the control, but were increased compared to the IP waves. Thus, modulus of elasticity values was similar to the control, though the Poisson's ratio for both varied from the control and each other. This difference in Poisson's ratios may be attributable to the difference in wave shape parameters or partial delamination noted above. Digital image correlation utilized from different angles may assist in determining the root of these effects in further testing.

Significant decreases in ultimate strength and strain at failure were noted in the OP2A and OP4A groups when tested in compression. Calculated modulus of elasticity was decreased in each case and the Poisson's ratios appear dubious further suggesting delamination and preventing conclusive determination of material properties. While it may appear that the delamination issue yielded results dissimilar to those found in blade sections, any of the assumption cases reviewed for scaling the OP waves would have resulted in variation from blade sections. Thus, these data are useful in the initial steps of building analytical models to match these material behaviors and provide a stepping stone to blade section analysis which will remove assumptions made during scaling.

v. Fiber misalignment

It is important to note that the parameters for both IP and OP waves were the same; amplitude and wavelength. Analysis of the results was performed to see if either parameter directly contributed to changes in ultimate stress. As noted by visual inspection of Figure 37 and Figure 38, there is not a strong correlation to either of these parameters which confirms previous research noted above. However, when correlating maximum fiber angle from each wavelength and amplitude combination (Figure 39), there appears to be an interesting trend closely approximating previous research.[41] In the cases of the 0° tension groups, the trend matches very closely with the exception of the low values associated with OP1. The 0° compression groups appear to be slightly anomalous in that ultimate stress increases slightly after an initial decrease. These variations are slight and appear to be the result of the delaminations noted above as the OP results appear to be causing the low points in the correlation. In short, these results confirm that as fiber misalignment angle of 0° laminates increases strength decreases.

As might be expected from the results of the IP waves noted above, the ±45° groups with higher fiber angles increased in ultimate stress. It is very interesting to noting that the ±45° tension groups had very little variation between any of the groups tested. This indicates that failure was the result of edge effects and the included defects did little to reduce ultimate stress. This is a further indicator that like the ±45°groups in compression, the ±45° groups in tension need no further analysis.

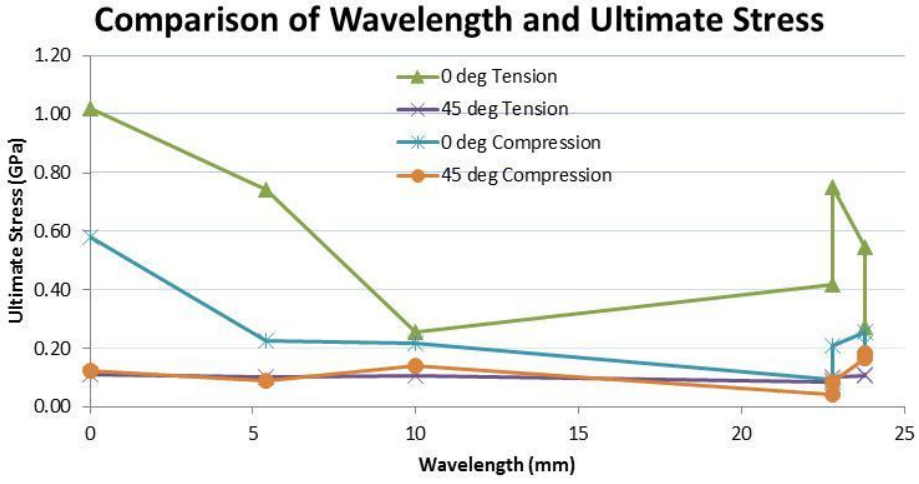

Figure 37: Comparison of wavelength and ultimate stress for each of the groups tested.

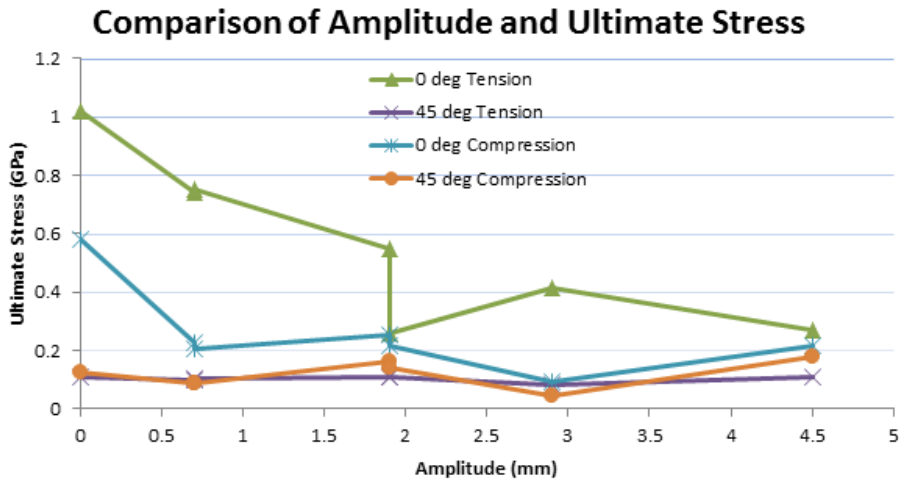

Figure 38: Comparison of amplitude and ultimate stress for each of the groups tested.

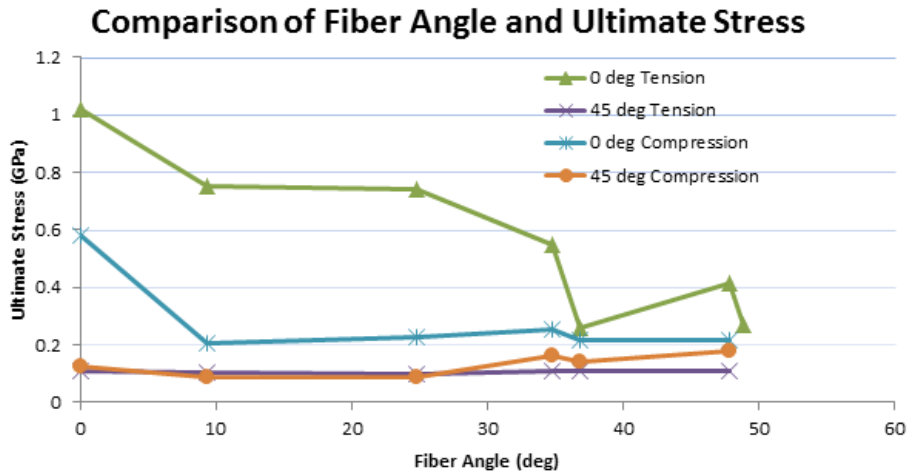

Figure 39: Comparison of fiber angle and ultimate stress for each of the groups tested.

vi. Round 1: Physical Testing Conclusions

Static test results have been presented from approximately 135 tests including four test groups, each of different defect type, in both tension and compression. Testing parameters for each of the defect types were determined as part of the Flaw Characterization study and were representative of wind turbine blade laminates with scaling as necessary for coupon level testing. In general, the static testing performed has allowed for initial analysis and will allow for convergence points for initial analytical models. Use of the digital image correlation system allowed for confirmation of the calculated strain and damage progression through strain field measurement during testing. Damage progression was found to vary for each defect type, but was found to generally involve matrix cracking, ply delamination, load redistribution and ultimately ply failure. Review of the manufacture of several of the sample types was deemed necessary, but only if additional testing at this scale is found to necessary once the modeling of this testing is completed.

More specifically, the following conclusions were reached:

1. Porosity was found to have a similar decrease in tensile strength (93% of control) compared to previous research even though this previous research was not performed utilizing specific wind turbine blade materials.
2. IP waves included in 0° laminates resulted in decreasing tensile properties (54-25% of control) as fiber misalignment angle increased.
3. IP waves of similar fiber misalignment angle, but different amplitude and wavelength, were found to have similar changes in tensile material properties (25-27% of control).
4. IP waves in ±45° laminates indicated an increase in compressive strength (112-133% of control). This observation may be due to the fibers in the wave approaching 0° and, therefore, an increased load carrying ability.
5. OP testing was hampered by delamination of the wave forms utilized, however, the data will be useful in initial modeling as any assumption set in scaling down to the coupon size would have been problematic or unrepresentative of blade laminates.
6. Independently amplitude and wavelength are insufficient for wave characterization.
7. Strength decreases (74-25% of control) with the increase of fiber misalignment angle (9-48°, respectively) within 0° laminates.
8. Due to the strength remaining static or increasing, the ±45° groups may be excluded from further testing.

D. Round 1: Modeling

i. Background and Methods

As noted, these results will be utilized for material properties and convergence points in building analytical models. Based on the research performed by Chang and Lessard, Abaqus has created a user subroutine to model damage progression for a circular hole within a composite laminate that achieves in good agreement.[42,45] Given that material properties degrade to zero upon reaching stress that induce a particular failure mode, this method is acceptable for comparison to this initial round of testing but is not applicable beyond this initial round. Efforts have been made to reach agreement utilizing this simplified modeling technique and will be traded for more robust methods in future rounds. This method modifies the nodal forces of an element of a composite material as damage accumulates and maps damage initiation and propagation when utilizing a micromechanics based failure criteria.[43]

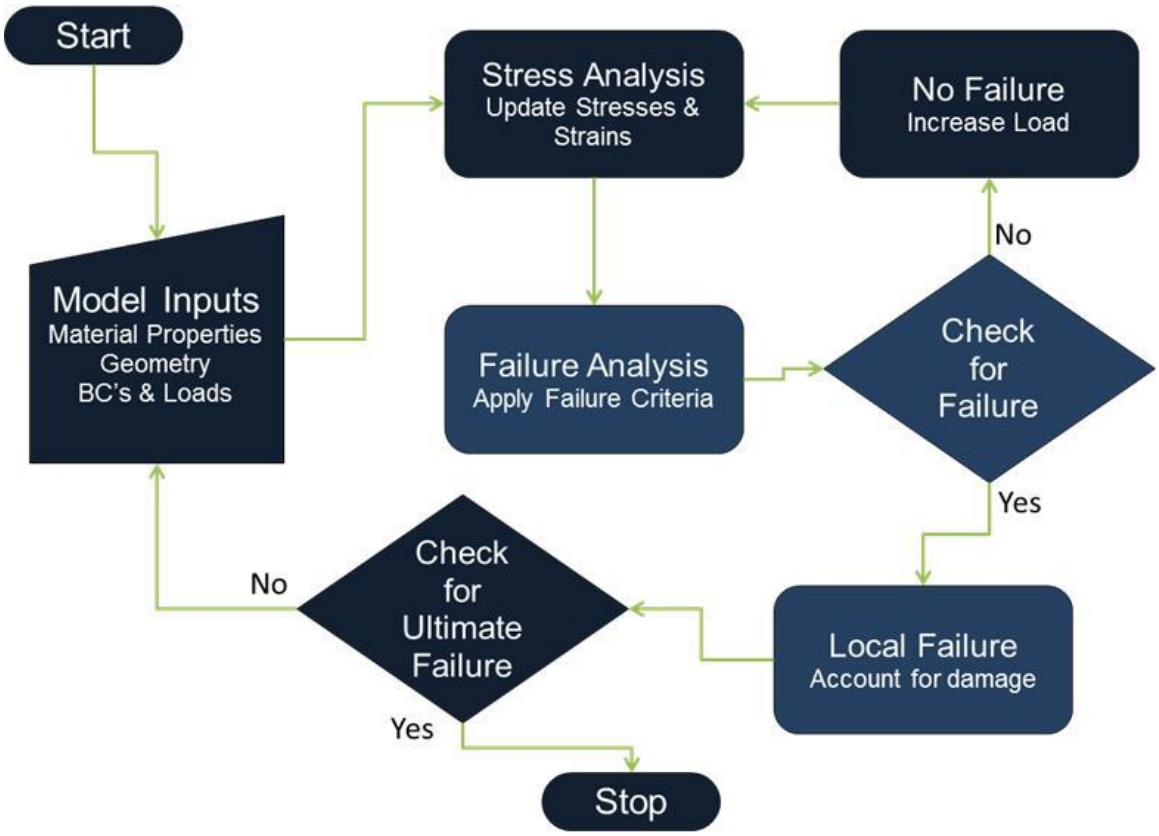

Figure 40: Decision tree for progressive damage modeling utilized in this round of modeling.

As outlined above, the damage progression model followed the decision tree shown in Figure 40 above. Several code files were written to run this model in Abaqus and the decision tree indicates the loops that are standard inputs (darker backgrounds) and user subroutines (lighter). In short, the standard input file build and meshes the model, while the user subroutine checks for damage at each step. If damage is detected, the material properties are adjusted or the loop is stopped if ultimate failure has occurred. In this case, matrix tensile cracking, matrix compressive failure, and fiber-matrix shearing failure are considered and the following failure indices are utilized[45]:

$$e_m^2 = \left(\frac{\sigma_y^{(i)}}{Y_t}\right)^2 + \frac{2\left(\sigma_{xy}^{(i)}\right)^2/G_{xy} + 3\alpha\left(\sigma_{xy}^{(i)}\right)^4}{2S_C^2/G_{xy} + 2\alpha S_C^4} \quad \text{if} \quad \sigma_y^{(i)} > 0 \tag{3}$$

$$e_m^2 = \left(\frac{\sigma_y^{(i)}}{Y_c}\right)^2 + \frac{2\left(\sigma_{xy}^{(i)}\right)^2/G_{xy} + 3\alpha\left(\sigma_{xy}^{(i)}\right)^4}{2S_C^2/G_{xy} + 2\alpha S_C^4} \quad \text{if} \quad \sigma_y^{(i)} < 0 \tag{4}$$

$$e_{fs}^2 = \left(\frac{\sigma_x^{(i)}}{X_c}\right)^2 + \frac{2\left(\sigma_{xy}^{(i)}\right)^2/G_{xy} + 3\alpha\left(\sigma_{xy}^{(i)}\right)^4}{2S_C^2/G_{xy} + 2\alpha S_C^4} \tag{5}$$

If damage is detected but not ultimate failure, the material properties are degraded to zero depending on the type of failure occurring. This is outlined in Table 8[25] below. As each of the failure indices above is calculated to be one (1), failure has occurred in that element and the material properties are adjusted based on the failure type. For example, if a matrix failure occurs, the failure indices included in the user subroutine result in failure value 1 (FV1) going from 0 to 1. As a result, the elastic properties for that

element only include E_x and G_{xy} as these are fiber dominated. The loop continues with the degraded properties until ultimately fiber failure has occurred.

Table 8: Material property degradation utilized in this round of modeling.

Material State	Elastic Properties				FV1	FV2	FV3
No failure	E_x	E_y	ν_{xy}	G_{xy}	0	0	0
Matrix failure	E_x	0	0	G_{xy}	1	0	0
Fiber/matrix shear	E_x	E_y	0	0	0	1	0
Shear damage	E_x	E_y	ν_{xy}	0	0	0	1
Matrix failure and fiber/matrix shear	E_x	0	0	0	1	1	0
Matrix failure and shear damage	E_x	0	0	0	1	0	1
Fiber/matrix shear and shear damage	E_x	E_y	0	0	0	1	1
All failure modes	E_x	0	0	0	1	1	1

ii. Model Set-up

The initial configurations utilized to work toward testing and modeling correlation were the Control and IP Wave 1. This wave form was modeled as a 2D surface utilizing the parameters noted in the Flaw Characterization portion above. The surface was then imported into Abaqus and the mesh was generated utilizing four layers (0.0375 in) of a quadrilateral, plane stress shell element (S4R). A displacement condition was applied to the top of the sample and the bottom was constrained. In addition, material properties and estimated strength properties were used along with local material coordinate systems through the wave of IP1. It must be noted that two IP1 waves were modeled due to the discrepancy between the intended and actual waves noted above. The intended wave form is labeled as IP1, while the actual is labeled as IP1_ACTUAL.

In reviewing the test data, images and DIC data, it was apparent that initial damage occurred in each of the wave samples at low loading levels on the ends of the samples where fibers ended on the sample edge (Figure 41). Due to the wave pattern introduced, when the samples were cut fibers through the wave were cut resulting in discontinuous fibers along the sample length. Based on this observation, it was assumed that these portions of the laminate were not of interest when considering the goal of isolating defects in this initial round. Thus, the geometry shown in Figure 42 was utilized for all of the IP1 modeling efforts herein while similar models with differing geometries were utilized for the Control and IP1_ACTUAL.

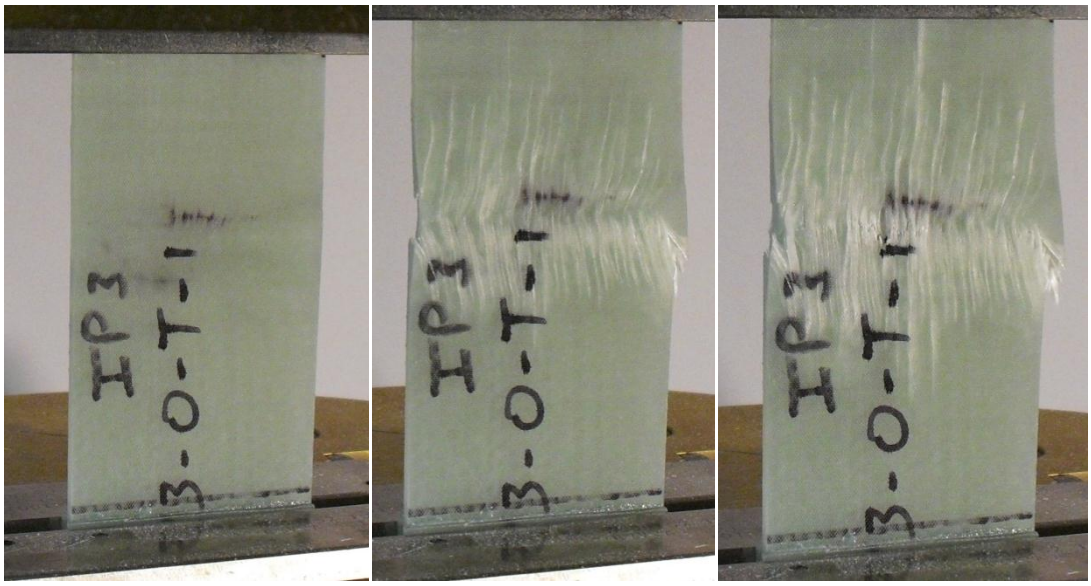

Figure 41: Damage progression of IP Wave 1 with initial damage accumulating at the areas where fibers are not continuous through the length of the sample.

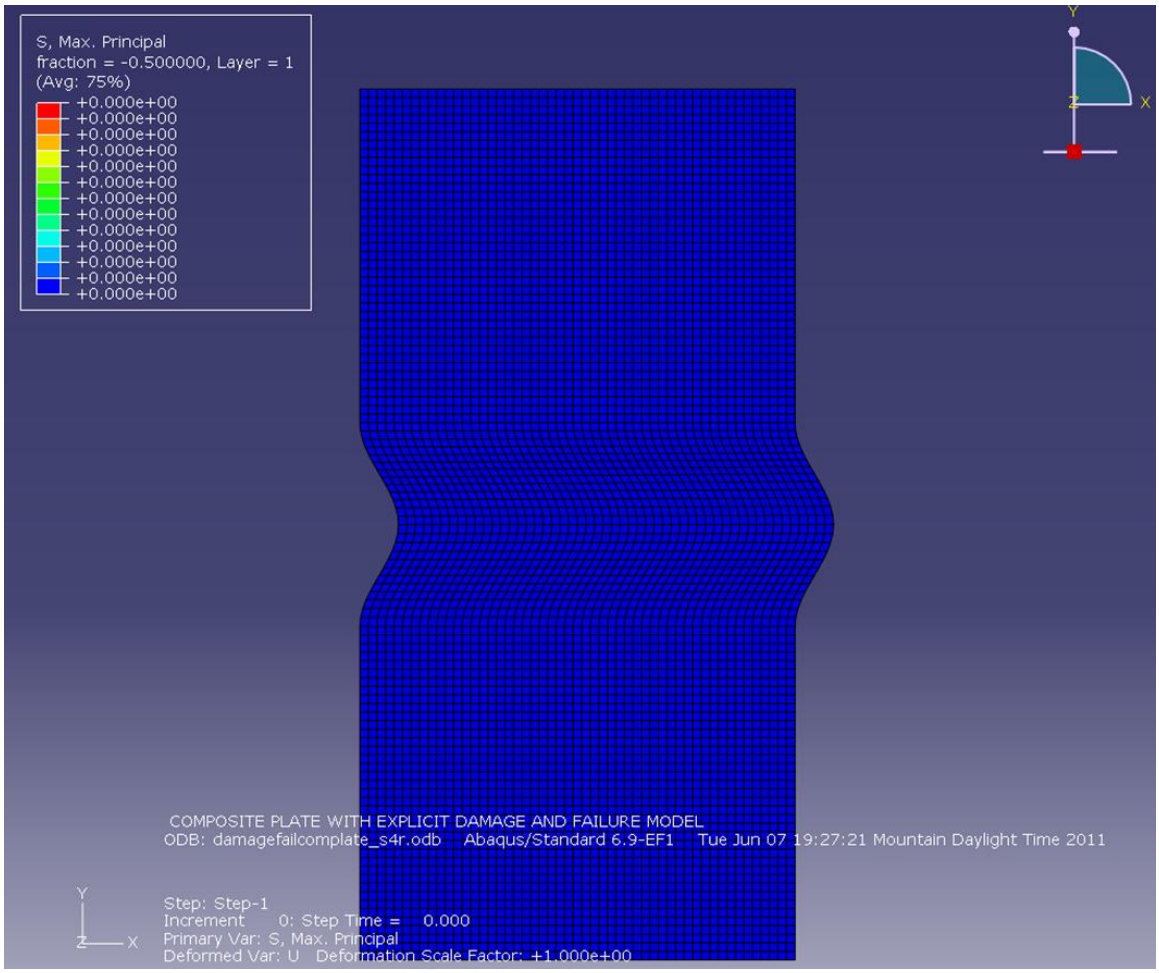

Figure 42: Meshed IP Wave 1 as model in Abaqus.

iii. Results and Discussion

As these were the first modeling efforts of this research, several steps were taken to ensure proper details were being considered and check for convergence. First, damage was checked for and the damage progression for IP1 is shown in Figure 43 below. Note that stress accumulates rapidly in the peak of the wave and increases until fiber-matrix failure and then with each step the damaged area grows. This matches the damage progression noted visually (Figure 41) and with the DIC (Figure 34).

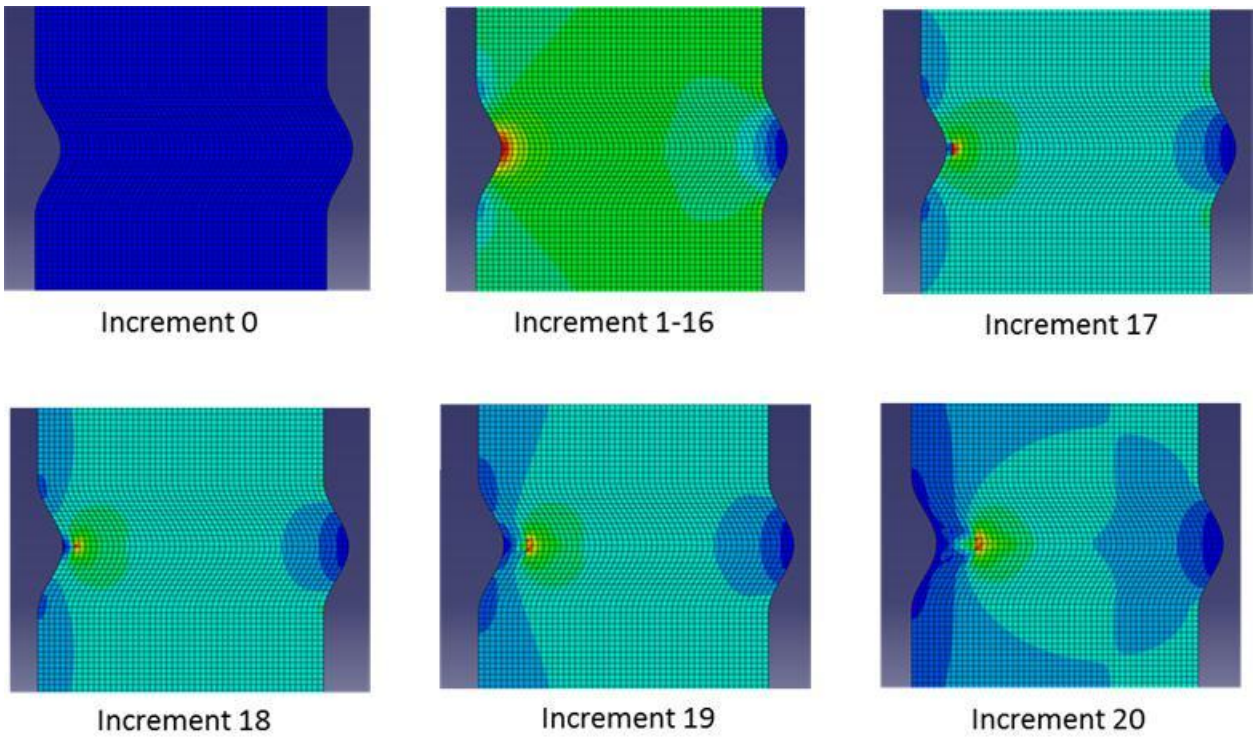

Figure 43: Modeled damage progression through time in a laminate with IP1.

All Control and IP Wave 1 models were tested in a linear elastic fashion to ensure the boundary conditions and model integrity. The load-displacement results of these models are compared to those from the physical testing below in Figure 44 and Figure 45. The dots in each graph are utilized to indicate the linear elastic models and show decent agreement with the elastic portion of respective test data. Once this agreement was achieved, the damage progression subroutine was turned on again and the results are also shown below. In the case of the Control, damage is predominantly fiber-matrix and occurs catastrophically at just over 40 kips which is in relative agreement with the physical test data.

The IP1 with damage progression initially showed reasonable agreement with the as-tested group though it overestimated the initial damage point. It appeared that significant changes to the elastic or strength properties were necessary to achieve agreement. However, once the actual wave pattern that was tested was also modeled, agreement improved. Further analysis of the estimated strength properties is necessary to improve agreement. Additional next steps to continue to improve these models are outlined below. It is worth noting that models for the ±45° control group were run and reasonable agreement was achieved through the elastic region of the linear elastic model. However, the damage progression subroutine utilized was not sufficient for matching the damage progression of the as-tested specimen. Thus, these partial results were not included in this report.

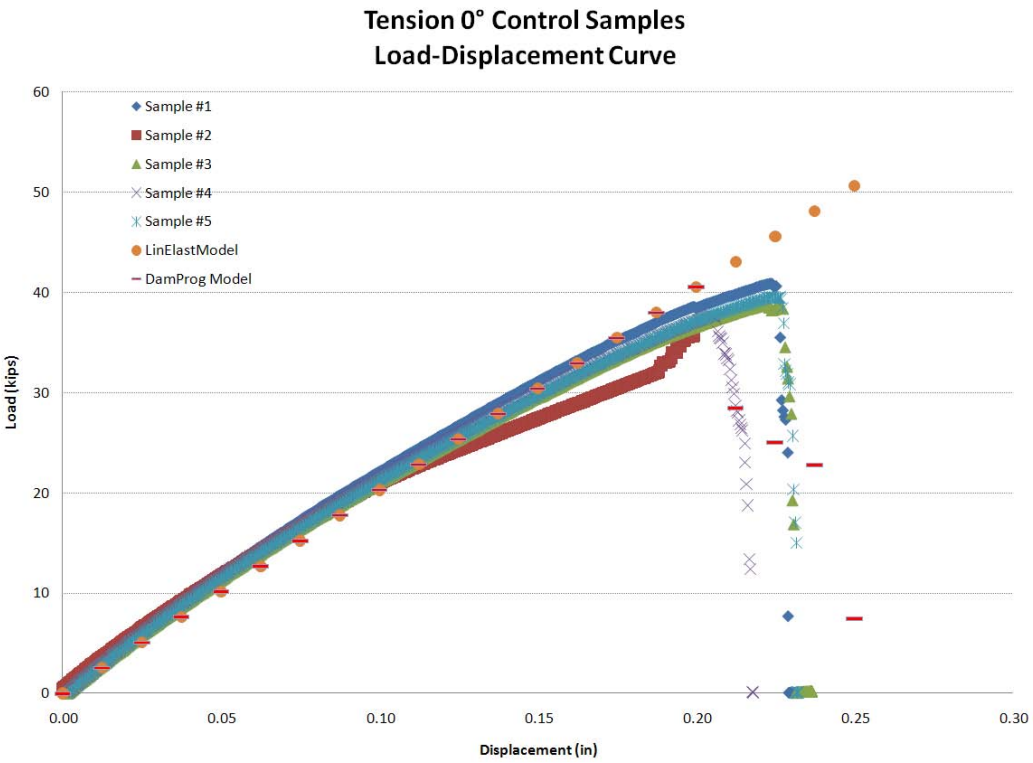

Figure 44: Comparison of 0° tension Control specimen results of load-displacement curves from physical testing and modeling.

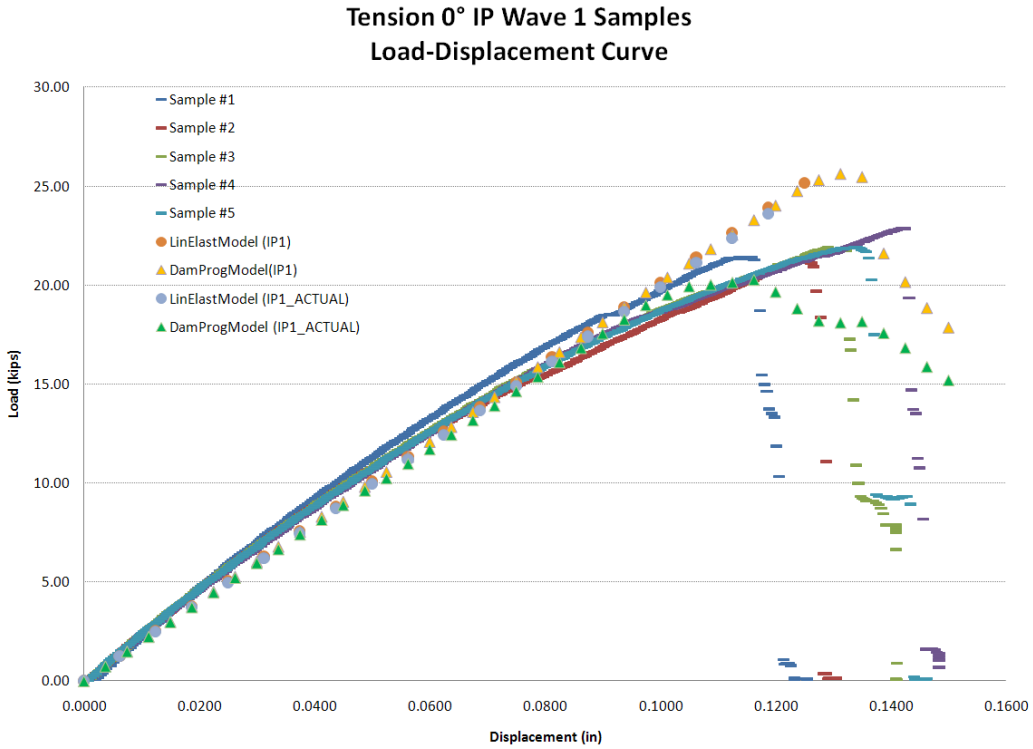

Figure 45: Comparison of 0° tension IP1 specimen results of load-displacement curves from physical testing and modeling.

iv. Modeling Next Steps

Even though these initial modeling efforts showed reasonable agreement, this simple model needs to be improved before it can be considered fully functional. A total of three rounds of effects of defects testing will be completed, and the modeling effort is continuous through all three rounds working toward better prediction at larger scales. Below is a list of each of the items to aid in finalizing this portion of the modeling effort, which allows for stepping toward more complex modeling efforts.

- Update and run models for other tested configurations
- Understand damage type for each model
- Compare to strains from model to DIC data and calculated stresses from test data
- Modify mesh size and element type to determine sensitivity to each
- Test sensitivity to oriented properties
- Update/add failure criteria and improve strength properties accuracy to improve damage progression subroutine

IV. Future Work

A. Round 2 Test Plan

1. Focus more heavily on improving analytical models; experimental efforts to support and improve models.
2. Manufacture and test samples of increased size and thickness compared to Round 1, but of a scale that is still testable at MSU. Ensure that samples tested match more closely defects observed in manufactured blades.
    a. Porosity: Try to investigate several laminates at higher volume percentage.
    b. IP waves: Improve layer consistency.
    c. OP waves: Improve manufacturing process to more accurately match defects observed in blades.
3. Add angled layers to laminate to provide confidence in multi-layer damage progression analytical and experimental correlations.
4. Elimination of all ±45° laminates from further testing as results from Round 1 indicate that in most cases defect laden samples were not significantly degraded compared to controls. Whereas, 0° laminates were worst-case for all defect types and therefore warrant the full focus of this investigation.
5. Improve damage progression visualization for comparison with analytical models. Utilize CT scans throughout loading to visualize damage progression through the thickness. Utilize DIC to visualize damage progress on surface.

B. Flaw Characterization

1. Continue to acquire as-built flaw data. Include more information such as flaw locations, and per blade distributions.
2. Research reliability methods suitable for wind turbine composites. Examples include the First Order Reliability Method, the β-Method, Response Surface Method and Taguchi Methods.
3. Refine criticality analysis algorithm and expand to include item 2, damage progression analysis as developed by Effects of defects and probability of detection criteria as developed by D. Roach at Sandia.
4. Characterize second round test specimen for use in model validation.

C. Effects of Defects

1. Work with current models toward improved convergence with test data.
    a. Update and run models for other tested configurations.
    b. Understand Damage type for each model.
    c. Compare to strains from model to DIC data and calculated stresses from test data.
    d. Modify mesh size and element type to determine sensitivity to each.
    e. Test sensitivity to oriented properties.
    f. Update/add failure criteria and improve strength properties accuracy to improve damage progression subroutine.
2. Research improved model types.
3. Once best convergence with current model is achieved move to more accurate model type.
4. Work with both model types to predict Round 2 test results.

References

[1]Hill, R. R., Peters, V. A., Stinebaugh, V. A., and Veers, P. S., "Wind Turbine Reliability Database Update," Sandia SAND2009-1171, 2009.

[2] Red, C., "Wind turbine blades: Big and getting bigger," *Composites Technology* (online journal) June, 2008, URL: http://www.compositesworld.com/articles/wind-turbine-blades-big-and-getting-bigger

[3]Walford, C. A., "Wind Turbine Reliability: Understanding and Minimizing Wind Turbine Operation and Maintenance Costs," Sandia SAND2006-1100, 2008.

[4]Veldkamp, D., "A Probabilistic Evaluation of Wind Turbine Fatigue Design Rules," *Wind Energy,* No. 11, 2008, pp. 655–672.

[5]Nelson, J.W., Riddle, T.W., & Cairns D.S. (2011). Characterization of Manufacturing Defects Common to Composite Wind Turbine Blades: Effects of Defects. *AIAA SDM Conference Denver*; April 2011.

[6] Adams, D. O., & Bell, S. J. (1995). Compression strength reductions in composite laminates due to multiple-layer waviness. *Composites science and technology , 53*, 207--212.

[7]Adams, D. O., & Hyer, M. (1993). Effects of layer waviness on the compression strength of thermoplastic composite laminates. *Journal of reinforced plastics and composites , 12*, 414.

[8]Argon A. S., "Statistical aspects of fracture," *Composite Materials*, Vol. 5, Fracture and Fatigue, 1974. pp. 153-190.

[9]Wagner H. D., "Statistical concepts in the study of fracture proper-ties of fibres and composites," *Application of Fracture Mechanics to Composite Materials*. 1989, pp. 39-77.

[10]Zweben C., "Is there a size effect in composites?," *Composites*, Vol. 25, 1994, pp. 451-454.

[11] Wisnom M. R., "Size effects in tensile, compressive and inter-laminar failure of unidirectional composites," ASME Aerospace Divisions, AD-Vol. 55, 1997. pp. 67-77.

[12] Wisnom, M. R., "Size effects in the testing of fibre-composite materials," *Composites Science and Technology* Vol. 59, 1999, pp. 1937-1957.

[13] Weibull W., "A statistical distribution function of wide applicability," *Journal of Applied Mechanics* Vol. 18, 1951, pp. 293-297

[14] Griffin, D. A., Ashwill, T. D., "Alternative composites materials for megawatt-scale wind turbine blades: Design considerations and recommended testing," *AIAA SDM Conference*, 2003

[15] Bar-Cohen, Y. "Emerging NDE Technology and Challenges at the beginning of the 3rd Millennium," *Material Evaluation,* Vol. 58, 2008, No. 1, pp. 17-30

[16] Ochoa, O. "Non-destructive Evaluation (NDE) Methods for Inspecting the Integrity of Composite Structures in the Offshore Oil Industry", *NDE Composites Workshop*, November 21, 2002

[17] Shapurian, T., Damoulis, P. D., Reiser, G. M., Griffin, T. J., Rand, W. M., "*Quantitative evaluation of bone density using the Hounsfield index*," The international journal of oral and maxillofacial implants, Vol. 21, 2006, No. 2, pp. 290-298

[18] "Procedures for performing a failure mode, effects and criticality analysis," Military Standard MIL-STD-1629A, 1980

[19] "Failure modes, effects and criticality analysis (FMECA) for command, control, communications, computer, intelligence, surveillance, and reconnaissance (C4ISR) facilities," Department of Army Technical Memorandum TM 5-698-4, 2006

[20]SANDIA Blade Reliability Collaborative Meeting Conversation, August 2010, Albuquerque, NM.

[21]Riddle, T.W., Cairns D.S. & Nelson, J.W. (2011). Characterization of Manufacturing Defects Common to Composite Wind Turbine Blades: Flaw Characterization. *AIAA SDM Conference Denver*; April 2011.

[22]Judd, N. C., & Wright, W. W. (1978). Voids and their effects on the mechanical properties of composites- an appraisal. *Sampe Journal , 14*, 10-14.

[23]Baley, C., Davies, P., Grohens, Y., & Dolto, G. (2004). Application of interlaminar tests to marine composites. A literature review. *APPLIED COMPOSITE MATERIALS , 11*.

[24]ZHU, H., LI, D., ZHANG, D., WU, B., & CHEN, Y. (2009). Influence of voids on interlaminar shear strength of carbon/epoxy fabric laminates. *Transactions of Nonferrous Metals Society of China , 19*, 470--475.

[25]Wisnom, M. R., Reynolds, T., & Gwilliam, N. (1996). Reduction in interlaminar shear strength by discrete and distributed voids. *Composites science and technology , 56*, 93--101.
[26]Wu, Y. N., Shivpuri, R., & Lee, L. J. (1998). Effect of macro and micro voids on elastic properties of polymer composites. *JOURNAL OF REINFORCED PLASTICS AND COMPOSITES , 17*.
[27]Guo, Z.-S., Liu, L., Zhang, B.-M., & Du, S. (2009). Critical Void Content for Thermoset Composite Laminates. *JOURNAL OF COMPOSITE MATERIALS , 43*.
[28]Pradeep, D., Reddy, N. J., Kumar, C. R., & Srikanth, L. (2007). Studies on mechanical Behavior of glass epoxy composites with induced defects and correlations with NDT characterization parameters. *JOURNAL OF REINFORCED PLASTICS AND COMPOSITES , 26*.
[29]Costa, M. L., de Almeida, S. F., & Rezende, M. C. (2005). Critical void content for polymer composite laminates. *AIAA JOURNAL , 43*.
[30]Adams, D. O., & Bell, S. J. (1995). Compression strength reductions in composite laminates due to multiple-layer waviness. *Composites science and technology , 53*, 207--212.
[31]Adams, D. O., & Hyer, M. (1993). Effects of layer waviness on the compression strength of thermoplastic composite laminates. *Journal of reinforced plastics and composites , 12*, 414.
[32]Bogetti, T. A., Gillespie, J. W., & Lamontia, M. A. (1994). The influence of ply waviness with nonlinear shear on the stiffness and strength reduction of composite laminates. *Journal of Thermoplastic Composite Materials , 7*, 76.
[33]Mandell, J. F., Samborsky, D. D., & Sutherland, H. J. (1999). Effects of materials parameters and design details on the fatigue of composite materials for wind turbine blades., (pp. 628--633).
[34]Wang, L. (2001). *Effects of In-plane Fiber Waviness on the Properties of Composite Materials.* PhD Thesis, Montana State University.
[35]Mandell, J., Samborsky, D., & Wang, L. (2003). Effects of Fiber Waviness on Composites for Wind Turbine Blades., (pp. 2653--2666).
[36]Avery, D. P., Samborsky, D. D., Mandell, J. F., & Cairns, D. S. (2004). Compression strength of carbon fiber laminates containing flaws with fiber waviness.
[37] Mandell, J. F., & Samborsky, D. D. (1997). *DOE/MSU composite material fatigue database: test methods, materials, and analysis.*
[38]ASTM D3039. *Standard test method for tensile properties of polymer matrix composite materials* .
[39]ASTM D3410-87. *Standard Test Method for Compressive Properties of Unidirectional or Cross-ply Fiber Resin Composites, American Society for Testing and Materials* .
[40]ASTM D3518. *Standard Test Method for In-Plane Shear Response of Polymer Matrix Composite Materials by Tensile Test*.
[41]Barbero, E. J. (1999). Introduction to composite materials design. *JOURNAL OF COMPOSITES FOR CONSTRUCTION* , 151.
[42]Chang, F. K. & Chang, K. Y. (1987) A Progressive Damage Model for Laminated Composites Containing Stress Concentrations. *Journal of Composite Materials*, v21, 834-855.
[43]Chang, F. K., & Lessard, L. B. (1991). Damage tolerance of laminated composites containing an open hole and subjected to compressive loadings. I: Analysis. *Journal of Composite Materials , 25*, 2-43.
[44]Evcil, A. (2008) Simulation of Three Dimensional Progressive Damage in Composite Laminates. *Intl Journal of Mechanics*, v2, 67-75.
[45]Tay, T. E., Tan, V. B. C., & Tan S. H. N. (2005). Method for Progressive Damage in Composite Structures. *Journal of composite Materials*, *39*, 1659-1675.
[46]Abaqus 6.9, Example Problem 1.1.14: Damage and failure of a laminated composite plate. Simulia, Providence, RI.

Appendix

A1. Flaw Characterization Figures

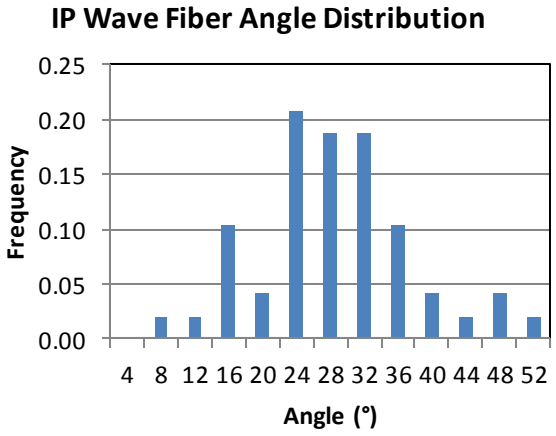

Figure 46: IP fiber angle distribution.

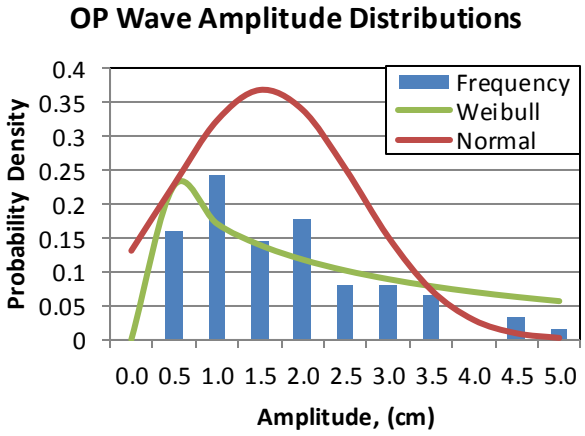

Figure 47: OP amplitude distributions.

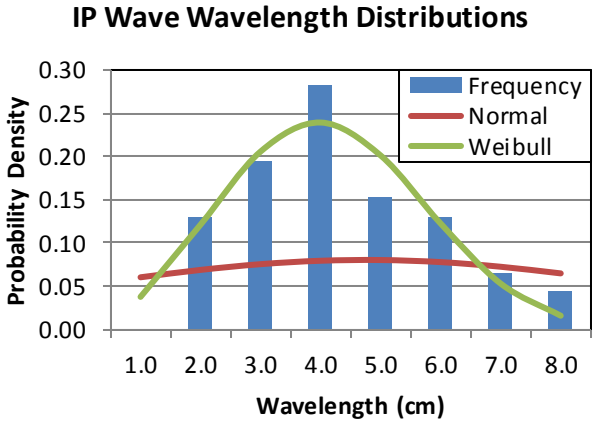

Figure 48: IP wave wavelength distributions.

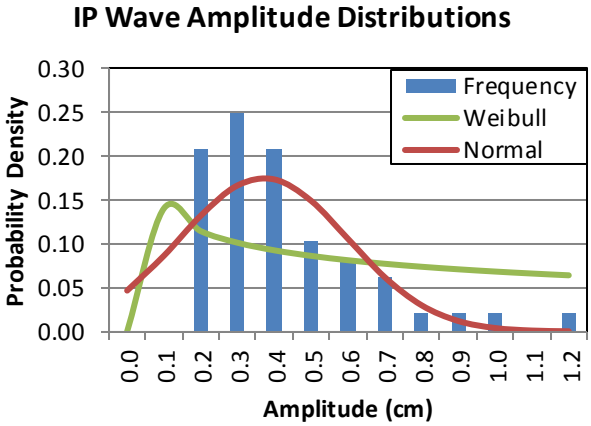

Figure 49: IP amplitude distributions.

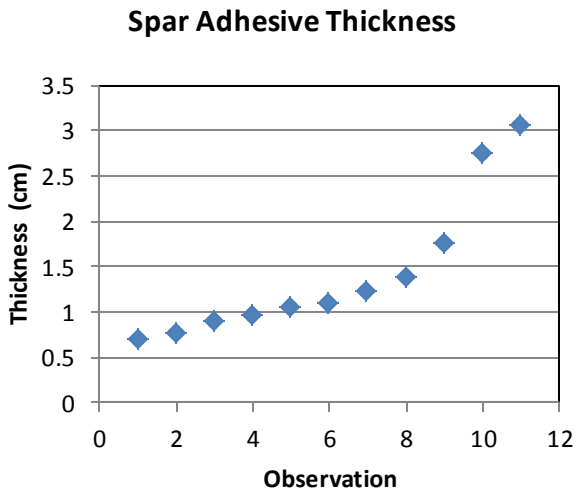

Figure 50: Adhesive bond thicknesses for spar/sheer web to blade skin.

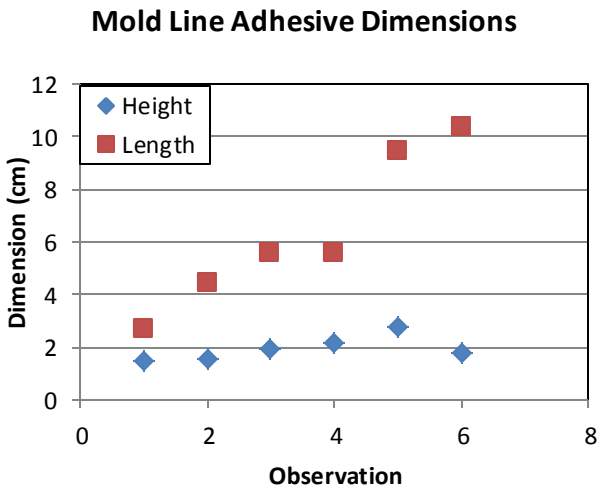

Figure 51: Adhesive layer dimensions for the mold line case.

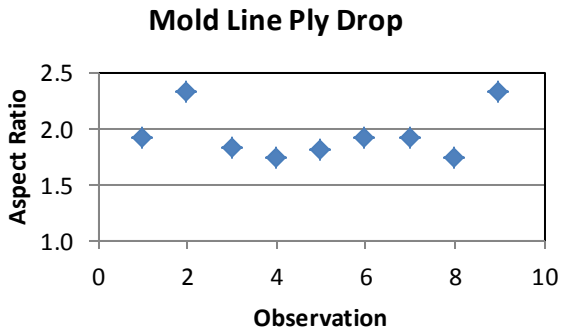

Figure 52: Adhesive layer dimensions for the mold line case.

A2. Criticality Analysis Case Study

Turbine Capacity (kW) =	1500.00
Blade Length (m) =	42.00
Porosity Content (%/100) =	0.02

These are global blade properties which are used to set up the analysis. Also included in this designation would be the materials used in blade construction such that the proper materials properties may be utilized in the analysis.

Item #	Type	Size Parameter 1: Width, Wavelength, % Porosity	Size Parameter 2: Height, Amplitude	Size Parameter 3: Fiber Angle	Location Parameter 1: LP, HP[3]	Location Parameter 2: Designation[4]
101	IP	3.66205	0.29	24.75	HP	Root Spar
102	IP	2.35545	0.24	29.05	LP	Root Skin
103	IP	2.85368	0.25	22.73	HP	Transition Spar
104	IP	3.57214	0.35	30.19	LP	Transition Skin
105	IP	26.11728	1.18	12.87	HP	Flap Spar
106	IP	3.60872	0.43	33.50	LP	Flap Skin
107	IP	1.95104	0.24	36.87	HP	Root Spar
108	IP	5.05840	0.94	50.66	LP	Root Skin
109	IP	1.98126	0.11	21.80	HP	Transition Spar
110	IP	5.17431	0.83	43.44	LP	Transition Skin
111	IP	3.78270	0.51	37.88	HP	Flap Spar
112	IP	6.07394	0.65	34.51	LP	Flap Skin
113	IP	5.71317	0.36	20.39	HP	Root Spar
114	IP	4.92339	0.50	31.07	LP	Root Skin
115	IP	3.46116	0.33	30.33	HP	Transition Spar
116	IP	3.41231	0.65	47.16	LP	Transition Skin
117	IP	3.45244	0.35	31.16	HP	Flap Spar
118	IP	3.04688	0.39	34.02	LP	Flap Skin

Location Parameter (L)	Designation Modifier
Root Spar	0.95
Root Skin	1
Transition Spar	0.5
Transition Skin	0.7
Flap Spar	0.7
Flap Skin	0.9

At present these are subjective modification factors. Future analysis will setup a quantitative designation.

In order to evaluate the strength of a flawed composite, simple regression models based on the experimental data collected in this investigation were generated to correlate ultimate strength with a flaw characterization parameter. For example purposes, only in-plane flaws and the off-axis fiber angle have been considered. The static mechanical test results and the corresponding correlations are shown

[3] The HP (high pressure) and LP (low pressure) parameters designate which mechanical property data set is used; tension and compression respectively.

[4] Generic description of the flaw location. Portions of the blade are designated based on their strain during loading

in the following two figures. These correlations are used in equation 3 to designate σ_f, the ultimate strength of a flawed laminate. Future analysis will incorporate more complex damage progression and/or residual strength models.

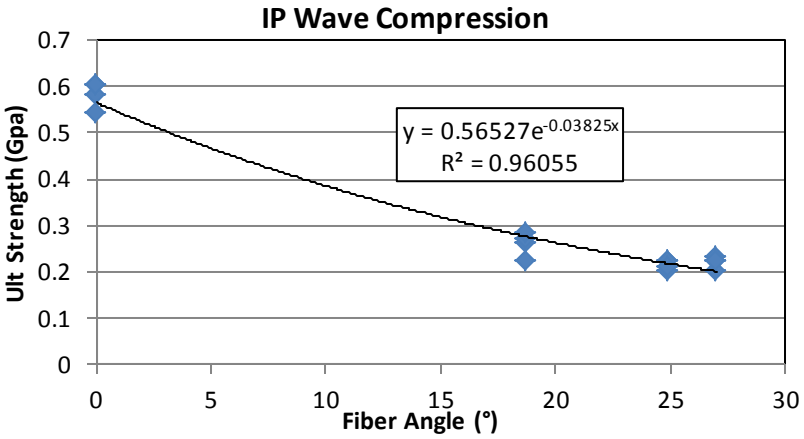

Figure 53: Example of mechanical response correlation between IP wave off-axis fiber angle and ultimate strength in compression

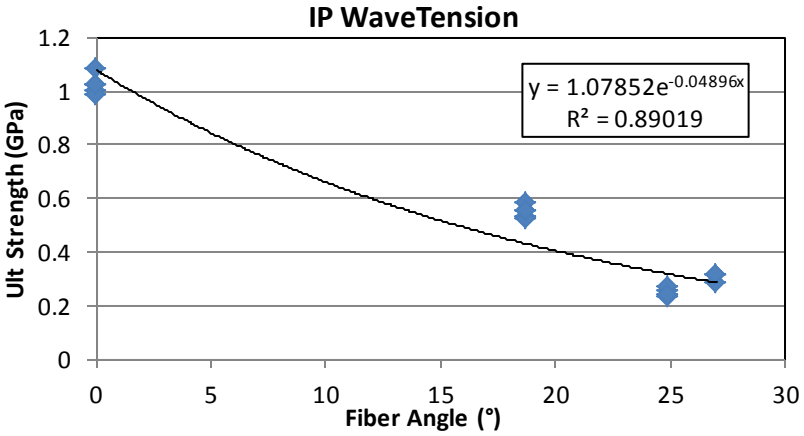

Figure 54: Example of mechanical response correlation between IP wave off axis fiber angle and ultimate strength in tension

Distribution:

Emily Baca (10)
Office of Wind and Hydropower Technologies
EE-2B Forrestal Building, U.S. DOE
1000 Independence Ave. SW
Washington, DC 20585

Doug Cairns (5)
Dept. of Mechanical & Industrial Engineering
Montana State University
PO Box 173800
320 Roberts Hall
Bozeman, MT 59717-3800

Paul Veers
NREL/NWTC
1617 Cole Boulevard MS 3811
Golden, CO 80401

Scott Hughes
NREL/NWTC
1617 Cole Boulevard MS 3811
Golden, CO 80401

Derek Berry
NREL/NWTC
1617 Cole Boulevard MS 3811
Golden, CO 80401

Steve Nolet
TPI Composites Incorporated
Structural Composites Division
373 Market Street
P.O. Box 367
Warren, RI 02885-0367

Internal Distribution:

MS1124 J. Berg, 6121 (Electronic)
MS 1124 S.M. Gershin, 6122 (Electronic)
MS 1124 D.T. Griffith, 6122 (Electronic)
MS 1124 B. Hernandez-Sanchez, 6122 (Electronic)
MS 1124 D. Laird, 6122 (Electronic)
MS 1124 B. LeBlanc, 6121 (Electronic)
MS 0615 S. Neigidk 6624
MS 1124 A. Ogilvie, 6121 (Electronic)
MS 1124 J. Paquette, 6121
MS 1124 M. Rumsey, 6121 (Electronic)
MS 0615 T. Rice, 6624
MS1124 B. Resor, 6121 (Electronic)
MS 0615 D. Roach, 6620
MS1124 J. White, 6121 (Electronic)
MS 1124 Wind Library, 6121 (5)
MS 0899 Technical Library, 9536 (electronic copy)

Sandia National Laboratories